the plant journal

SEB SOCIETY FOR EXPERIMENTAL BIOLOGY

The Plant Journal (2022) **110,** 1681–1699 doi: 10.1111/tpj.15764

The *cellulose synthase-like F3* (*CslF3*) gene mediates cell wall polysaccharide synthesis and affects root growth and differentiation in barley

Haoyu Lou[1,2], Matthew R. Tucker[1,*], Neil J. Shirley[1,3], Jelle Lahnstein[1,3,4], Xiujuan Yang[1], Chao Ma[1], Julian Schwerdt[1,4], Riccardo Fusi[2], Rachel A. Burton[1,3], Leah R. Band[2,5], Malcolm J. Bennett[2] and Vincent Bulone[1,3,4,6*]

[1]*School of Agriculture, Food and Wine, University of Adelaide, Waite Campus, Urrbrae, South Australia 5064, Australia,*

[2]*Division of Plant and Crop Sciences, School of Bioscience, University of Nottingham, Sutton Bonington Campus, Loughborough, Leicestershire LE12 5RD, UK,*

[3]*ARC Centre of Excellence in Plant Cell Walls, School of Agriculture, Food and Wine, University of Adelaide, Waite Campus, Urrbrae, South Australia 5064, Australia,*

[4]*Adelaide Glycomics, School of Agriculture, Food and Wine, University of Adelaide, Waite Campus, Urrbrae, South Australia 5064, Australia,*

[5]*School of Mathematical Sciences, University of Nottingham, Nottingham NG7 2RD, UK, and*

[6]*Division of Glycoscience, Department of Chemistry, School of Engineering Sciences in Chemistry, Biotechnology and Health, Royal Institute of Technology (KTH), AlbaNova University Centre, Stockholm, Sweden*

Received 11 November 2021; revised 4 April 2022; accepted 5 April 2022.; published online 8 April 2022.
*For correspondence (e-mails vincent.bulone@adelaide.edu.au; matthew.tucker@adelaide.edu.au).

SUMMARY

The barley *cellulose synthase-like F* (*CslF*) genes encode putative cell wall polysaccharide synthases. They are related to the *cellulose synthase* (*CesA*) genes involved in cellulose biosynthesis, and the *CslD* genes that influence root hair development. Although *CslD* genes are implicated in callose, mannan and cellulose biosynthesis, and are found in both monocots and eudicots, *CslF* genes are specific to the Poaceae. Recently the barley *CslF3* (*HvCslF3*) gene was shown to be involved in the synthesis of a novel (1,4)-β-linked glucoxylan, but it remains unclear whether this gene contributes to plant growth and development. Here, expression profiling using qRT-PCR and mRNA *in situ* hybridization revealed that *HvCslF3* accumulates in the root elongation zone. Silencing *HvCslF3* by RNAi was accompanied by slower root growth, linked with a shorter elongation zone and a significant reduction in root system size. Polymer profiling of the *RNAi* lines revealed a significant reduction in (1,4)-β-linked glucoxylan levels. Remarkably, the heterologous expression of *HvCslF3* in wild-type (Col-0) and root hair-deficient Arabidopsis mutants (*csld3* and *csld5*) complemented the *csld5* mutant phenotype, in addition to altering epidermal cell fate. Our results reveal a key role for *HvCslF3* during barley root development and suggest that members of the *CslD* and *CslF* gene families have similar functions during root growth regulation.

Keywords: Oroot development, cell wall, cellulose synthase-like gene, glucoxylan, *Hordeum vulgare*, barley, Arabidopsis.

INTRODUCTION

The plant cell wall plays an important role in the flexibility and stability of cell structures during root development (De Lorenzo et al., 2019; Houston et al., 2016). In addition, it is involved in the defence against pathogens and acts as a carbohydrate sink to meet the growth requirements of the plant (Tucker et al., 2018). The synthesis and composition of root cell walls are complex, as evidenced by the heterogeneity of Arabidopsis cell walls from different root tissues (Somssich et al., 2016). Cell wall polysaccharide synthesis and modification are the result of the action of glycosyltransferases (GTs), glycoside hydrolases (GHs), methyltransferases and acetylesterases (Lombard et al., 2014; Tucker et al., 2018). The products of the *cellulose synthase* (*CesA*) and *cellulose synthase-like* (*Csl*) genes belong to the large GT2 family (Lombard et al., 2014). Studies have shown that these genes are involved in the synthesis of various cell wall polysaccharides, including cellulose (*CesA*) (Doblin et al., 2002), (1,3;1,4)-β-glucan (*CslF*, *CslH*, *CslJ*) (Burton et al., 2006; Cseh et al., 2013; Doblin et al., 2009; Taketa

et al., 2011), mannan (*CslA*, *CslD*) (Dhugga et al., 2004; Goubet et al., 2009; Liepman et al., 2005; Verhertbruggen et al., 2011; Yin et al., 2011), callose (*CslD*) (Douchkov et al., 2016), (1,4)-β-linked glucoxylan (*CslF*) (Little et al., 2019), and xyloglucan (*CslC*) (Cocuron et al., 2007).

Gene expression profiling suggests that the *CslF* family might be involved in *Hordeum vulgare* (barley) root development. Indeed, quantitative PCR revealed high transcript levels of genes such as *HvCslF3* in rapidly growing organs, including root tips (Burton et al., 2008). Of the 10 *CslF* genes in the barley genome, only *HvCslF6* and *HvCslF9* have been studied *in planta* through mutagenesis and transgenic modification (Burton et al., 2011; Garcia-Gimenez et al., 2020; Taketa et al., 2011). *CslF6* fulfils a central role in the synthesis of (1,3;1,4)-β-glucan (Burton et al., 2006), whereas heterologous expression studies also suggest potential roles of other *CslF* genes in the synthesis of (1,3;1,4)-β-glucan (*CslF9*) (Cseh et al., 2013) and (1,4)-β-linked glucoxylan (*HvCslF3*, *HvCslF10*) (Burton et al., 2006; Little et al., 2019), although this has not been confirmed *in planta*.

Evolutionary studies revealed that the *CslF* subfamily is the sister clade to the *CslD* subfamily of genes, which in turn are homologous to the *CesA* genes (Richmond & Somerville, 2000; Schwerdt et al., 2015). Little et al. (2018) analysed 46 species and presented phylogenetic evidence that the *CslF* clade may have evolved from the *CslD* subfamily. Although the precise biochemical roles of individual *CslD* genes are yet to be assigned, the involvement of the *CslD* genes in the regulation of the synthesis of primary cell walls in rapidly growing tips of pollen tubes and root hairs has been described in diverse species, including Arabidopsis (Yin et al., 2011), *Oryza sativa* (rice) (Li et al., 2009) and *Populus trichocarpa* (poplar) (Peng et al., 2019). Among the four *CslD* genes present in barley, *HvCslD2* functions in pathogen defence through alterations of callose deposition and cell wall composition (Douchkov et al., 2016). Despite these results, it remains unclear whether barley *CslF* and/or *CslD* genes are involved in root growth. Their phylogenetic relationship and similar tendency to be highly expressed in roots provided impetus to assess their function in root development, with a particular focus on *HvCslF3*. Hence, we investigated whether functional and biochemical redundancy exists between *HvCslF3* and the Arabidopsis *CslD3* and *CslD5* genes. By using transgenic barley downregulated in *HvCslF3* expression and employing *HvCslF3* in complementation experiments of Arabidopsis *csld3* and *csld5* mutants, we demonstrate that *HvCslF3* expression is positively correlated with root elongation, cell radial patterning and (1,4)-β-linked glucoxylan accumulation in barley root tips. The successful phenotypic recovery of *csld5* by *HvCslF3* expression in Arabidopsis revealed that *HvCslF3* not only enhanced root hair growth and elongation, but also altered the fate of epidermal cells from non-hair cells to hair-forming cells.

RESULTS

Expression analysis reveals *HvCslF3* expression is elevated in outer root elongating tissues

Gene expression analysis (Figure 1) was performed on RNA collected from finely dissected wild-type (WT) *H. vulgare* cv. Golden Promise root tips representing the meristem (zone 1), elongation (zone 2), young maturation (zone 3) and old maturation (zone 4) zones (Figure 1a). Transcript levels of *HvCslF3* were determined by quantitative polymerase chain reaction (qPCR) (Figure 1e). *HvCslF3* was barely expressed in the meristem zone, but the transcript level increased dramatically and peaked in the elongation zone. As root cells enter maturation and start to differentiate, *HvCslF3* expression reduced to very low levels, as detected in zone 4. This expression pattern was distinct from that of *HvCslF6*, the expression of which was most abundant in the young and old maturation zones. The high expression of *HvCslF3* in the elongation zone suggested a potential role in cells that undergo rapid expansion.

To confirm the qPCR results and further investigate the location of gene expression, mRNA *in situ* hybridization was performed (Figure 1b–d). Longitudinal sections revealed that the expression of *HvCslF3* is elevated in epidermis and cortex cells in the elongation zone. Less intensive staining was observed in the central stele and meristem, with no staining in the root cap and mature cells surrounding the stele. These results were consistent with the qPCR analysis.

HvCslF3 is downregulated in root tips of barley 35S:*HvCslF3-RNAi* lines

To study the role of *HvCslF3* in barley, RNA interference (RNAi)-mediated gene silencing was used to generate transgenic plants with reduced *HvCslF3* gene expression. The RNAi plasmids were designed to target *HvCslF3*, with a 5′ untranslated region (5′-UTR) silencing fragment amplified from WT and driven by the constitutive *35S* promoter. A 35S:nlsYFP line confirmed that the promoter is active throughout the WT root tip (data not shown). Seeds from three independent homozygous *HvCslF3-RNAi* lines (#27, #29, #30) and WT plants were examined, and the expression level of *HvCslF3* in the first centimetre of the root tips was determined by qPCR. Figure 1(f) shows the fold change in transcript abundance of *HvCslF3* compared with the WT. The downregulation of *HvCslF3* was confirmed in all transgenic lines, although the degree of downregulation varied. Line #27 showed the most severe effect, retaining only 33.7% of WT *HvCslF3* expression. The transcript reduction in lines #29 (50.4%) and #30 (54.4%) was less severe compared with WT levels.

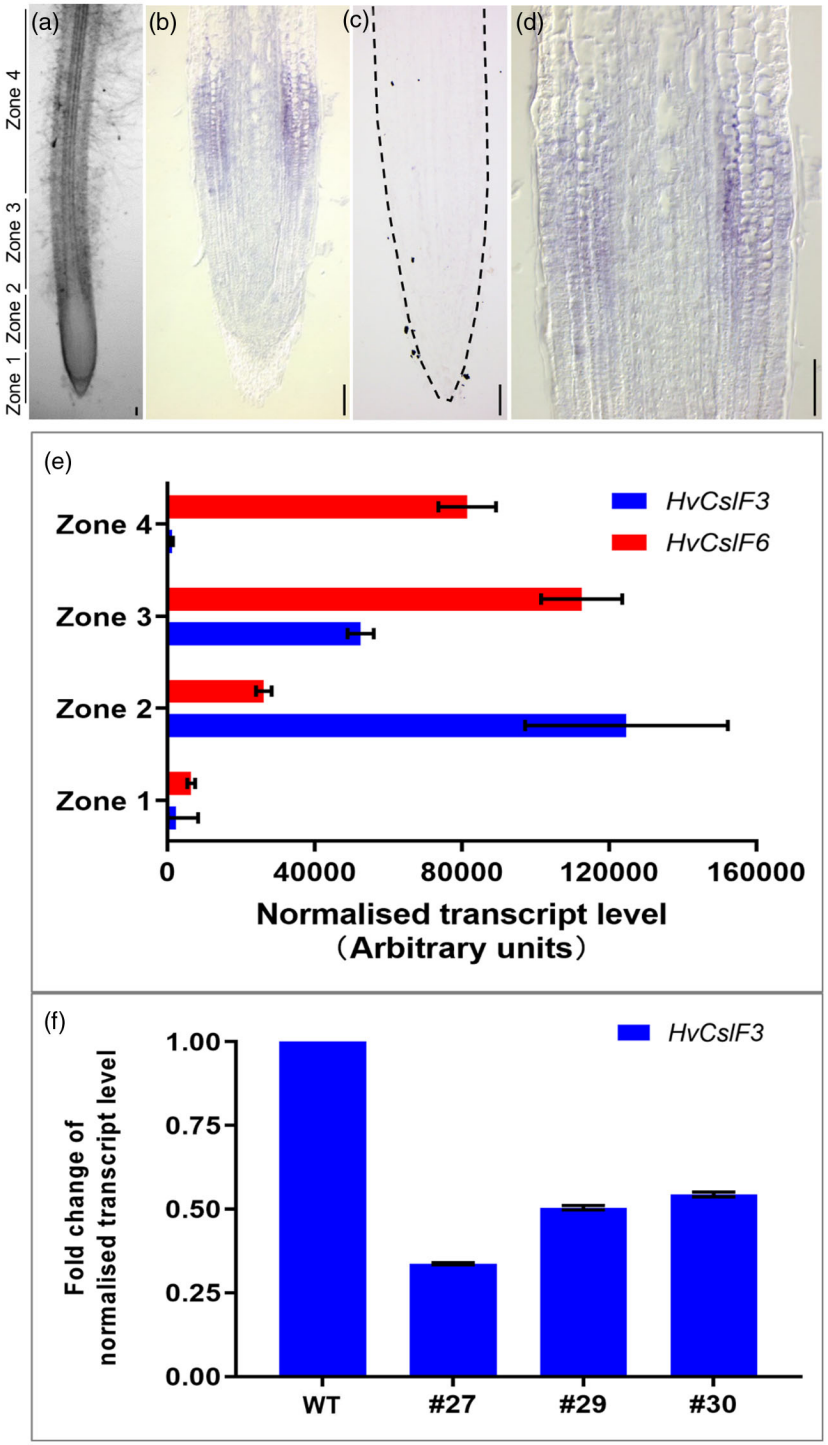

Figure 1. Gene expression analysis of *HvCslF3* in *Hordeum vulgare* (barley) root tip. (a) Schematic diagram of the regions used for root tip dissection and RNA collection. Zones 1, 2, 3 and 4 represent the root meristematic, elongation, young maturation and old maturation zones, respectively.
(b–d) mRNA *in situ* hybridization of *HvCslF3* using antisense (b, d) and sense (c) probes on longitudinal root sections.
(e) qPCR results showing the normalized transcript abundance of *HvCslF3* and *HvCslF6* in different zones of the root. Error bars indicate standard errors.
(f) Fold change of normalized transcript abundance of *HvCslF3-RNAi* barley lines compared with the wild type (WT). The level of downregulation was significant, with variability between each line ($P < 0.0001$). Scale bars: 100 μm.

HvCslF3 downregulation leads to changes in barley seedling root growth

Barley seedlings were germinated on 1% agar plates and root growth was assessed over time. Figure 2(a) shows representative 7-day-old seedlings, with the transgenic lines exhibiting generally smaller seedlings with a reduced root system. Interestingly, the total seminal root length of line #27 was significantly reduced over the measuring period, whereas lines #29 and #30 had seminal root lengths that were similar to those of the WT from 4–5 days post-germination (4–5 dpg) onwards (Figure 2b). After germination, root length increased rapidly until 3 dpg with most of

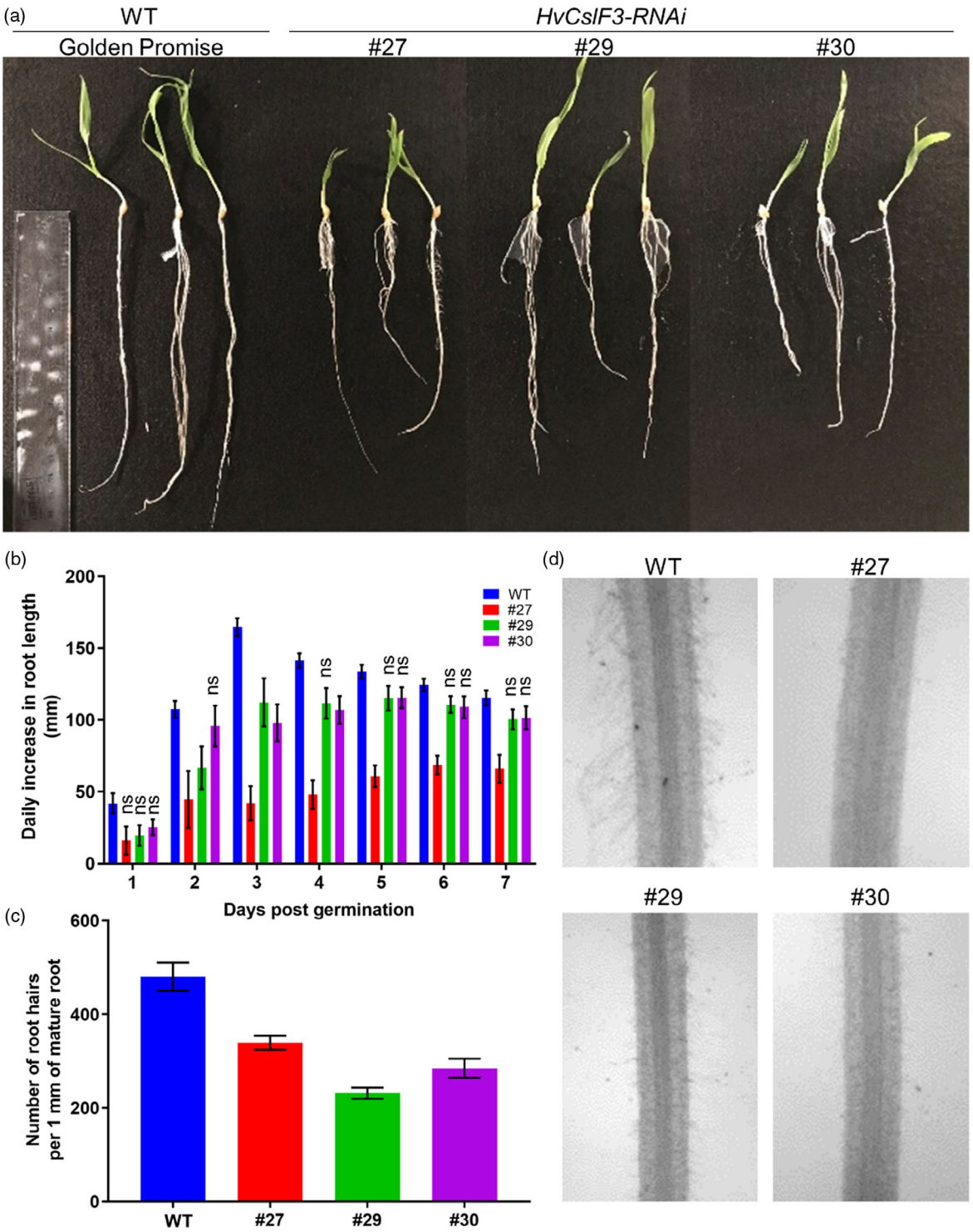

Figure 2. Variation in root morphology and development between the wild type (WT) and the *HvCslF3-RNAi* lines.
(a) Seedlings of WT and *HvCslF3-RNAi* lines (#27, #29, #30) at 7 days post-germination (7 dpg).
(b) The total length of elongated seminal roots was measured daily for 7 days. Data were collected from 12 seedlings per genotype. Error bars indicate standard errors. Significance was tested with two-way ANOVA; unless indicated, the treatments showed significant differences compared with the WT (ns, not significant).
(c) Average number of root hairs on mature roots collected from 5-dpg seedlings germinated in the dark. Data represent the average of 10 seminal roots collected from different seedlings. Error bars indicate standard errors.
(d) Light microscopy pictures of roots treated with Hoyer's solution.

the lines exhibiting the highest root growth rate. At 3 dpg, the seminal root length of line #27 increased by 42 mm, whereas the increase in root length in the WT was 165 mm. From 3 dpg onwards the daily seminal root growth in each line stabilized, with minor fluctuations, at 115–125 mm day^{-1} in WT, 60–68 mm day^{-1} in #27, 100–115 mm day^{-1} in #29 and 102–115 mm day^{-1} in #30. The restrictions on root system development of the *HvCslF3-RNAi* lines continued throughout plant vegetative growth up to 50 dpg (e.g. line #27 in Figure S1). Root bending sensitivity assays in which barley seedlings were rotated by 90° at 3 dpg revealed no defects in gravitropism between the WT and the *HvCslF3-RNAi* lines (Figure S2). Indeed, a similar increase of bending angle was observed in all lines throughout the time course of the experiment.

Notably, defects in development were not limited to seminal root length. Indeed, the number of root hairs on the root tips was also decreased. Figure 2(c) shows the average number of root hairs on every centimetre of mature root, with significant differences observed between the WT and transgenic barley plants. WT roots showed 481 ± 30 root hairs, whereas the transgenic lines had 340 ± 15 (#27), 232 ± 12 (#29) and 285 ± 20 (#30) root hairs. Moreover, the root hairs of the transgenic lines were particularly sensitive to treatment with chloral hydrate-based clearing solutions. Figure 2(d) shows cleared root samples treated with Hoyer's solution. Compared with the WT, damage and/or removal of root hairs from the root surfaces of the transgenic barley lines was more obvious, especially for line #27, where the root hairs were almost completely removed.

HvCslF3 RNAi lines exhibit a shorter elongation zone

To understand the basis of the observed defects in root development, root tips were cleared with a ClearSee solution to examine cellular organization. The anatomy of the root tips was similar to that previously described by Kirschner et al. (2017). However, differences in the length of the elongation zone were observed between the lines. To compare the size of the meristem and elongation zones, we identified the end of the meristem zone and the beginning of the elongation zone based on the criterion that the first cortex cell adjacent to the epidermis doubles in length, whereas the end of the elongation zone was marked where the first root hair emerges. Figure 3 highlights the lengths of the meristem and elongation zones from different lines. The average meristem length in Golden Promise is approximately 1070 μm, which is comparable with that previously described in 4-day-old Morex roots (1000 μm) (Kirschner et al., 2017). However, the meristem size of the *HvCslF3-RNAi* plants was more variable, ranging between 589 and 1027 μm. In addition, the size of the elongation zone of all transgenic lines showed a significant reduction compared with the WT (WT, 924 μm; #27, 324 μm; #29, 335 μm; #30, 358 μm). The reduced length of the elongation zone (Figure 3b) was correlated with the level of *HvCslF3* gene expression (Figure 1(f)). The number of cells in the elongation zone varied between each plant examined, but no significant differences were observed across the different barley lines (Figure 3c). The consequence of the elongation (and meristem) zone defect is likely to be a shorter root and slower root growth, consistent with the root measurements presented in Figure 2.

HvCslF3-RNAi lines develop narrower roots

A notable trend of narrower roots was observed in the transgenic *HvCslF3-RNAi* barley plants. Figure 4(a) shows representative root sections for each line at approximately 1 cm from the root tip. The size of the central stele of all samples was comparable with that of the WT (approx. 130–150 μm), suggesting that the decrease in root diameter was likely to result from the reduced area of outer tissues. Compared with the WT, which usually contains an average of five or six cortical cell layers, only three or four layers of cortical cells were found in transgenic lines, with no obvious change identified in cell size. Quantitative data also show a correlation between cortical cell number and cortical area, where the *HvCslF3-RNAi* plants presented variable but significant reductions in cortical area compared with the WT roots (Figure 4c). Furthermore, because the roots were thinner, the number of epidermal cells in *HvCslF3-RNAi* plants (80–90) was reduced compared with the WT (>100). Hence, the lower root hair density observed in transgenic lines might be indirectly linked to the decreased number of epidermal cells surrounding the reduced number of cortical layers.

The deposition and distribution of major cell wall polysaccharides are not significantly affected in *HvCslF3-RNAi* lines

HvCslF3 belongs to the *CslF* gene family, of which several members have previously been implicated in the biosynthesis of (1,3;1,4)-β-glucan (Burton et al., 2006; Taketa et al., 2011). However, most of these studies have focused on aerial organs rather than roots. The deposition of major cell wall polysaccharides, including (1,3;1,4)-β-glucan, arabinogalactan protein (AGP), arabinoxylan, callose, mannan and pectin, was analysed by immunolabelling to detect any possible effect of reduced *HvCslF3* expression on polysaccharide composition in barley root tips. Keeping in mind that these experiments are semi-quantitative at best – meaning that only marked differences are detected with this approach – the data obtained from multiple replicates suggest that there was no obvious difference in cell wall polysaccharide deposition and distribution between the WT and the mutants (Figure S3). In the sampled root tip specimens from different genotypes, (1,3;1,4)-β-glucan was found in all cell types above

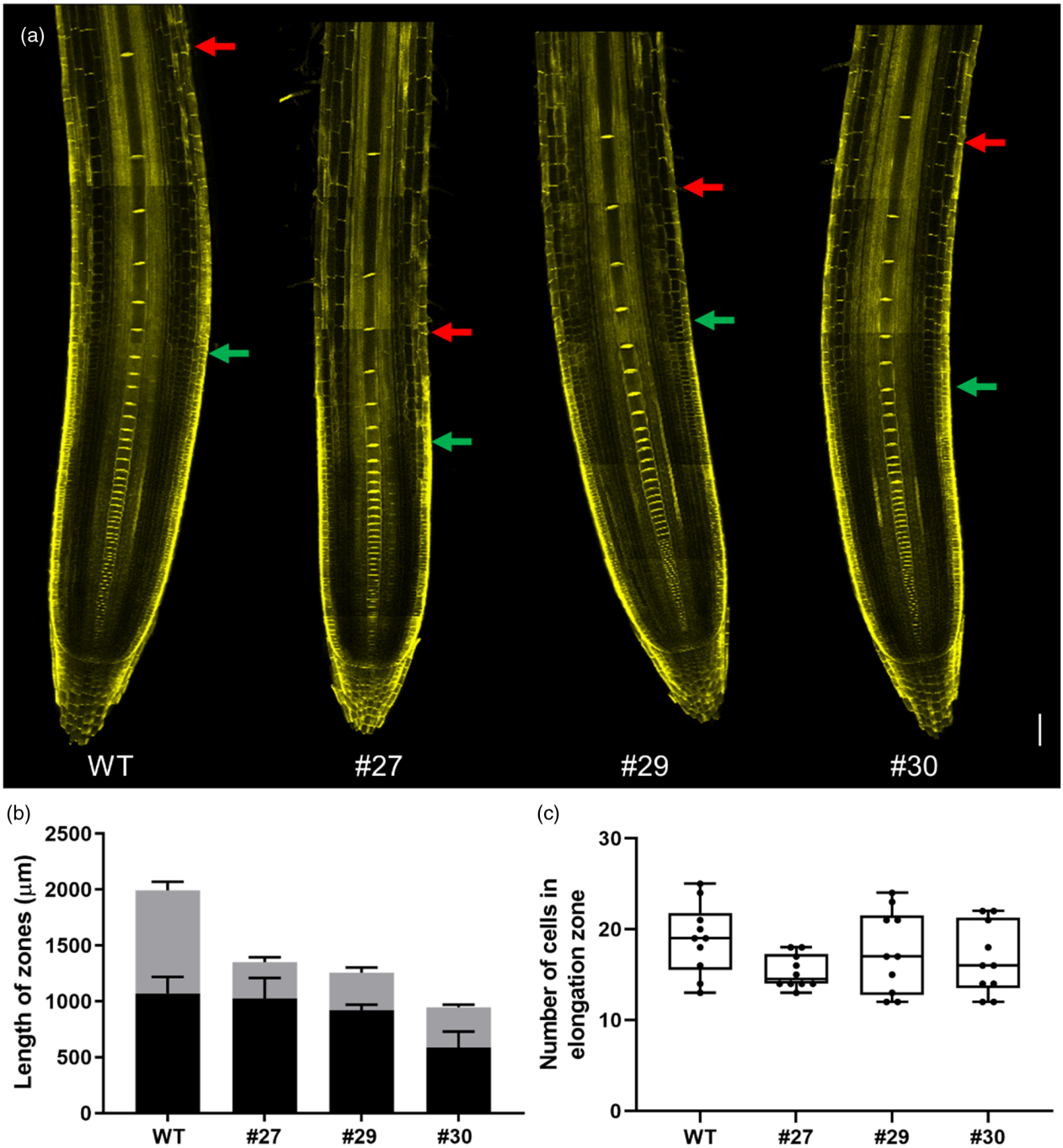

Figure 3. *HvCslF3-RNAi* plants develop shorter elongation zones.
(a) *Hordeum vulgare* (barley) root tips treated with ClearSee and Direct Yellow 96. Photos were taken with a Leica SP8 confocal microscope. Green arrows indicate the first cortical cell that doubles in length to mark the end of the meristematic zone and the beginning of the elongation zone, whereas red arrows indicate the first appearance of root hairs to mark the end of the elongation zone and the beginning of the maturation zone. Scale bar: 100 μm.
(b) Quantitative measurements of the sizes of the meristematic (black) and elongation (grey) zones. Similar meristematic zone sizes were observed in different genotypes, except for #30, which showed smaller meristematic size. A significant decrease of the elongation zone was observed in the *HvCslF3-RNAi* lines compared with the wild type (WT) ($P < 0.0001$). Error bars represent standard deviations.
(c) Number of cells in the elongation zones of the WT and mutant lines. Bars represent the maximum and minimum numbers recorded ($n = 10$).

the root cap, and the intensity of the labelling increased as cells leave the meristem zone. (1,3;1,4)-β-Glucan labelling in the root cap was restricted to the lateral root cap and young columella cells (Figure S3). The labelling was similar in both WT and mutant lines throughout the elongation to maturation zone. Another common

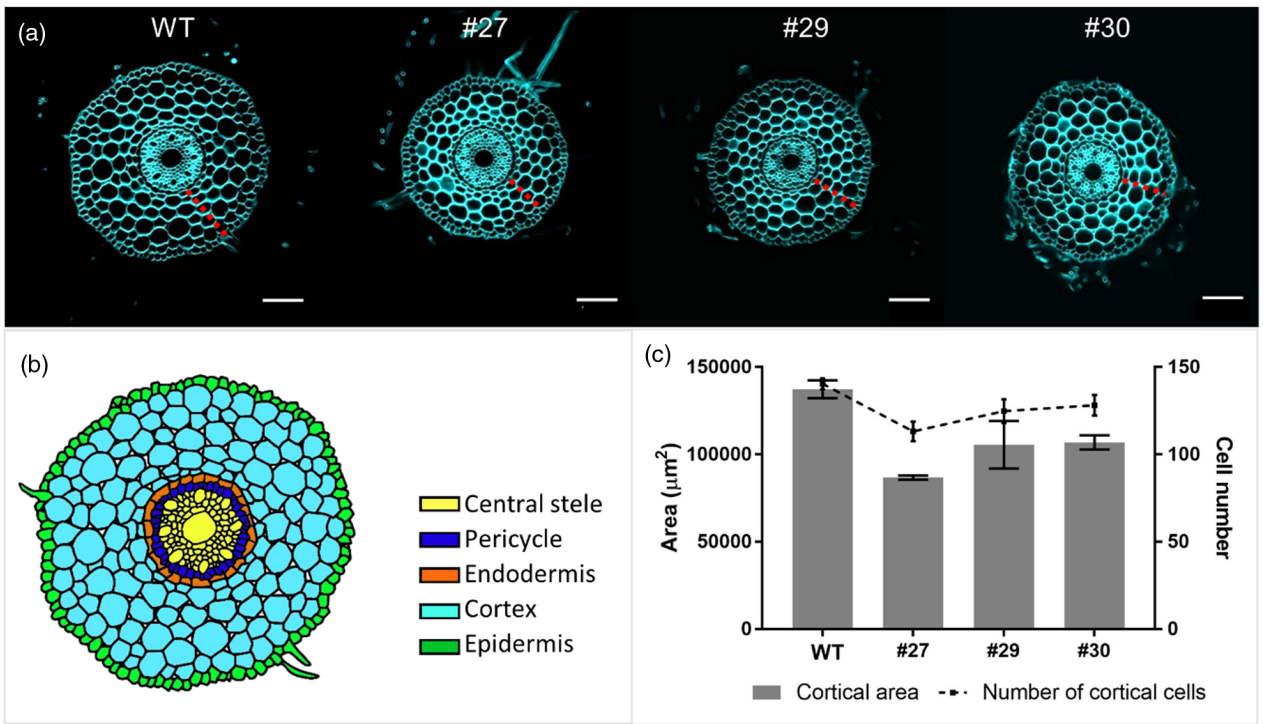

Figure 4. Transverse sections of *Hordeum vulgare* (barley) seminal roots.
(a) The wild type (WT) showed five or six layers of cortical cells, whereas the *HvCslF3-RNAi* lines showed approximately three or four cell layers (marked with red dashed lines). Sections of 100-μmthickness were taken at 1 cm from the root tip and stained with Calcofluor White. The images shown are representative of the photos of 10 individual specimens. Scale bars: 100 μm.
(b) Schematic diagram of the radial patterning of different cell types in a mature barley root.
(c) Quantitative measurements of root cortex. The *HvCslF3-RNAi* lines showed significantly reduced cortical area compared with the WT ($P < 0.0001$) (grey bars). The dashed line indicates a decreasing trend in the number of cortical cells in the transgenic barley lines, but no significant difference was observed between the cortical cell numbers. Error bars represent standard deviations.

polysaccharide, arabinoxylan, was not detectable in the walls of root tip cells (Figure S3).

Callose showed a change in deposition during root development (Figure S3). In the meristem, callose was detected in the cell plates of most cells but the labelling was less intense in the cells surrounding the stem cell niche and cells undergoing rapid cell division. In more mature cells, the callose signal was detected as bright punctate dots in the cell walls, demarking plasmodesmata. AGP was found in the cell walls of the central stele and outermost layer of the root cap, whereas pectin was restricted to cortex cells (Figure S3). Mannan showed a distinct localization compared with other polysaccharides, as fluorescent immunolabelling with anti-mannan antibodies was found in the cytoplasm, rather than at the cell walls. The fluorescent signal most likely corresponds to labelling in the Golgi apparatus; however, some non-specific labelling of other intracellular components cannot be ruled out. Similar labelling was identified when cells had entered a maturation phase, although the enlarging vacuole appeared to push the fluorescent signal towards the cell periphery, with the signal occasionally detected in the cell walls.

HvCslF3 downregulation reduces (1,4)-β-linked glucoxylan accumulation

The role of *HvCslF3* in the heterologous synthesis of (1,4)-β-linked glucoxylan in *Nicotiana benthamiana* (tobacco) leaves was recently described by Little et al. (2019). To assess the impact of reduced *HvCslF3* expression on endogenous (1,4)-β-linked glucoxylan levels in barley, root samples from the different transgenic lines were hydrolysed with the cellulase E-CELTR from *Trichoderma longibrachiatum* and oligosaccharide products were quantified by HPLC (Dionex) to determine (1,4)-β-linked glucoxylan concentration. Figure 5a shows the products from E-CELTR treatment, which are identified as xyl-(1,4)-β-glc, xylobiose, glc-(1,4)-β-xyl, and cellobiose, according to their retention times. Of these, xyl-(1,4)-β-glc and glc-(1,4)-β-xyl are the disaccharide products from hydrolysed (1,4)-β-linked glucoxylan. The sum of the disaccharides represents the level of (1,4)-β-linked glucoxylan (Figure 5b). On average, 1290 ng mg^{-1} of (1,4)-β-linked glucoxylan was detected in WT root tips, which was more than 10 times higher than previously detected in larger segments of barley root tissues (Little et al., 2019). Notably, the level of (1,4)-β-linked

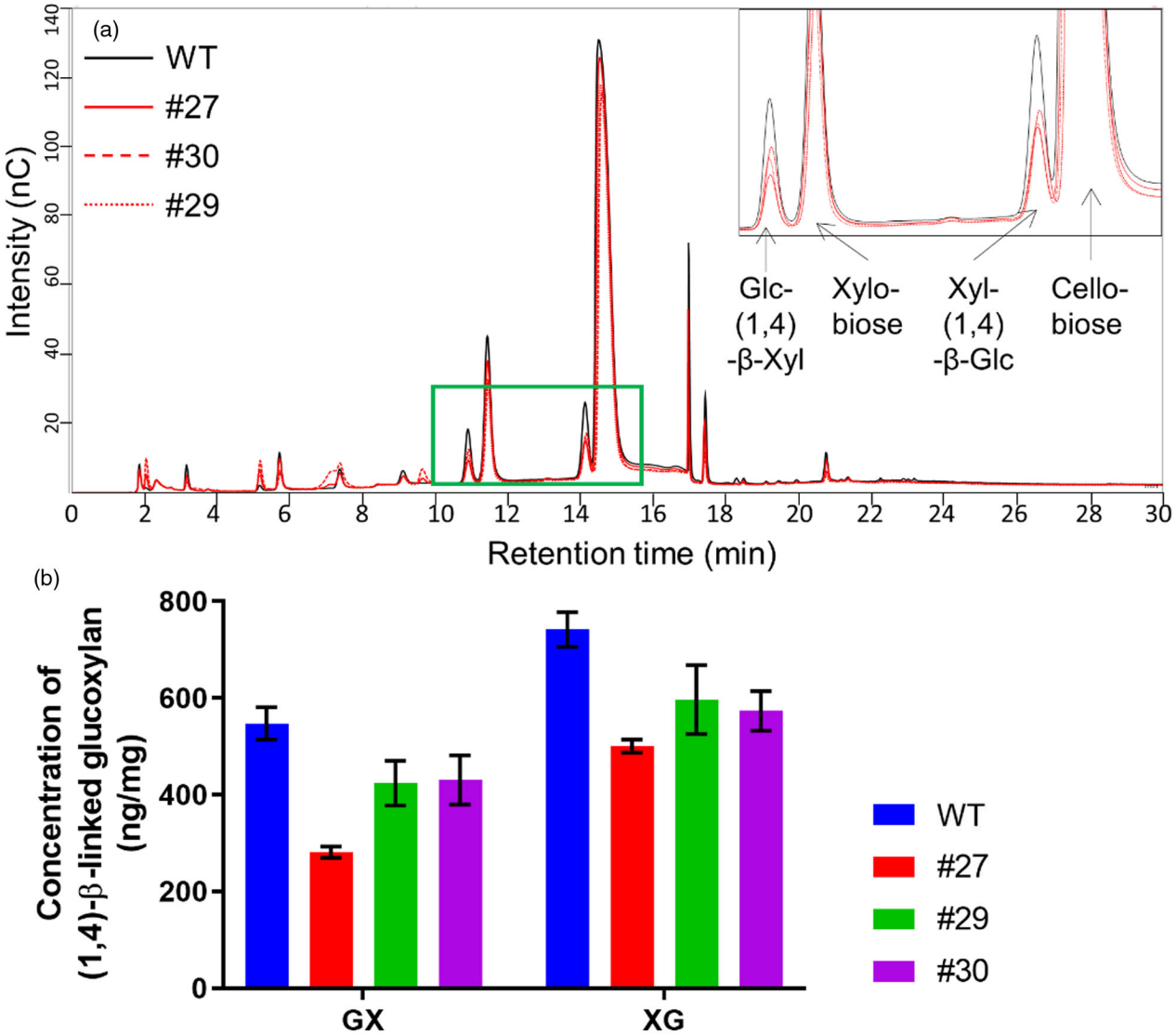

Figure 5. Quantification of (1,4)-β-linked glucoxylan in the root tips of wild-type (WT) and *HvCslF3-RNAi* plants. AIR root tissues were treated with the cellulase E-CELTR, and the hydrolysed clarified solutions were fractionated before HPLC analysis.
(a) Chromatogram of the hydrolysates. In the green box, peaks corresponding to glc-(1,4)-β-xyl, xylobiose, xyl-(1,4)-β-glc and cellobiose are indicated.
(b) Average concentration of glc-(1,4)-β-xyl (GX) and xyl-(1,4)-β-glc (XG) in root tips. Error bars represent standard errors. Significance was tested with two-way ANOVA; unless indicated, the treatments were significantly different from the WT.

glucoxylan in all three *HvCslF3-RNAi* lines was decreased significantly, showing average concentrations of 782, 1021 and 1004 ng mg^{-1} in lines #27, #29 and #30, respectively.

Expression of *HvCslF3* promotes root hair development in Arabidopsis

CslF and *CslD* gene families represent sister clades (Figure S4), although their evolutionary history remains to be fully resolved (Hazen et al., 2002; Little et al., 2018). The Arabidopsis genome lacks *CslF* genes and therefore provides an ideal heterologous expression model to study the function of *HvCslF3* during root development, both in the presence and absence of *AtCslD* genes. *HvCslF3* was transformed into WT Arabidopsis using a strong *Ubiquitin10* promoter for overexpression. Enhanced root hair growth was observed in transgenic Col-0 plants expressing *HvCslF3* (Figure 6a,d). The average length of mature root hairs in the Col-0¦pUbq10::HvCslF3 lines ranged from 0.41 to 0.56 mm, which was significantly longer than those observed in the Col-0 plants (0.22 mm) (Figure 7a). This suggests a potential role of *HvCslF3* in promoting root hair elongation.

In addition to the effects on root hair length, the root hair density was also increased in these transformed plants (Figure 7b). The average root hair number per millimetre of root was increased by 1.6-fold in the Col-0¦pUbq10::

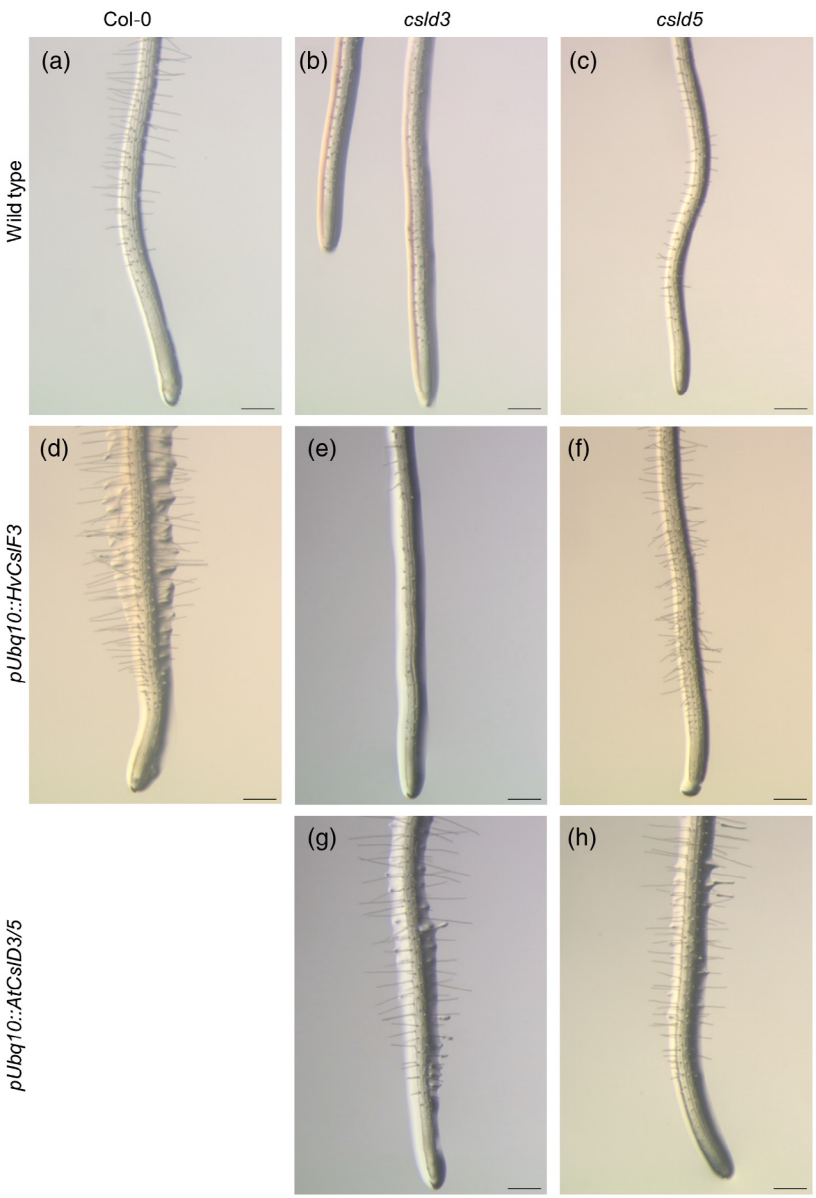

Figure 6. Arabidopsis root phenotypes of the complementation experiments with *HvCslF3, AtCslD3* and *AtCslD5* driven by the *Ubiquitin10* promoter. Roots were photographed from 7-day-old seedlings grown vertically on half-strength MS medium under controlled conditions in a growth chamber.
(a) Col-0 wild-type (WT) Arabidopsis root tips.
(b) *csld3* mutant showing aborted or abnormal root hair growth.
(c) *csld5* mutant showing short and disrupted root hairs.
(d) Col-0 expressing *HvCslF3* showing enhanced root hair growth.
(e) *HvCslF3* expression in *csld3* mutant, showing that the mutant phenotype was not restored.
(f) *HvCslF3*-complemented *csld5* mutant with restored root hair development.
(g) *AtCslD3*-complemented *csld3* mutant with recovered root hair phenotype.
(h) *AtCslD5*-complemented *csld5* mutant with recovered root hair phenotype. Scale bars: 0.5 mm.

HvCslF3 plants, consistent with the finding of reduced root hair density in the *HvCslF3-RNAi* lines. The seedling materials of three independent homozygous events were also collected to analyse their cell wall composition. In the Col-0 plants, (1,4)-β-linked glucoxylan was barely detectable (Figure S5). Out of the two expected oligosaccharides, only glc-(1,4)-β-xyl showed a very weak signal on the spectrometer, whereas the other oligosaccharide xyl-(1,4)-β-glc was undetectable. This suggests that no (1,4)-β-linked glucoxylan was found in the cell walls of WT Arabidopsis seedlings. Curiously, no differences in the abundance of either oligosaccharide were induced by the overexpression of *HvCslF3* (Figure S5). This contrasts with the findings of Little et al. (2019) who suggested a direct connection between the *HvCslF3* gene and the biosynthesis of (1,4)-β-linked glucoxylan in transformed tobacco leaves.

HvCslF3 rescues the *Atcsld5* root hair mutant phenotype

In Arabidopsis, defective root hair elongation was observed in *csld3* and *csld5* mutants, as previously reported by Yin et al. (2011) and shown in Figure 6(b,c). Considering the close phylogenetic relationship between the *CslF* and *CslD* families, and the gain-of-function phenotype observed for *HvCslF3* in Col-0 plants, we expressed *HvCslF3* in both *csld3* and *csld5* mutant backgrounds to examine the possibility of functional complementation. As expected, the aborted root hair phenotype in *csld3* was successfully recovered in transgenic plants expressing

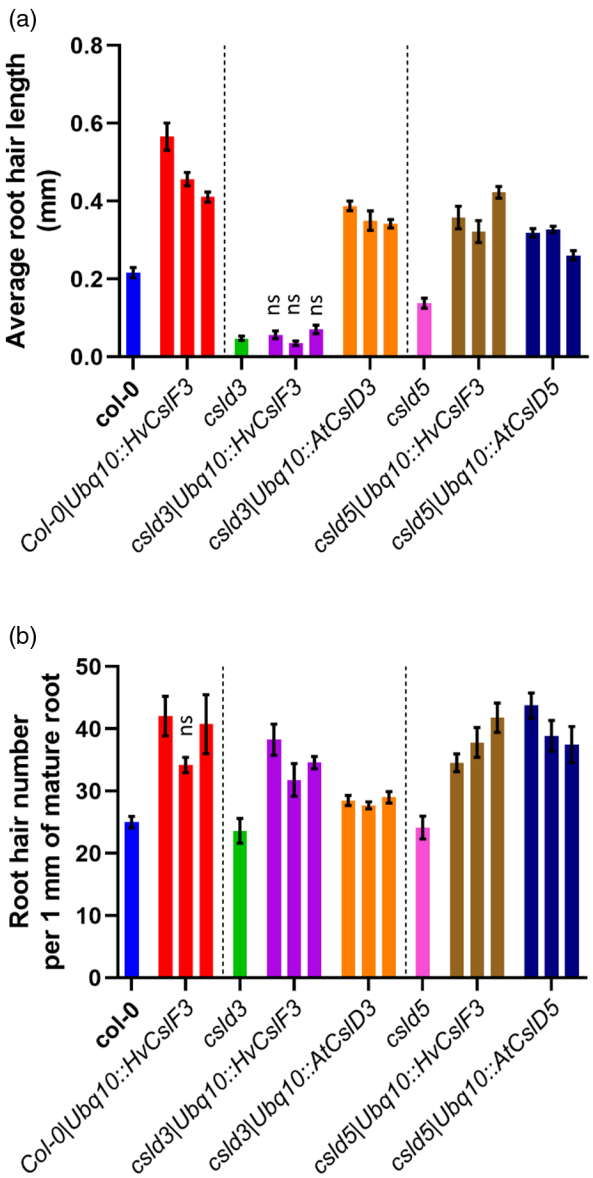

Figure 7. Quantification of root hair length (a) and density (b) in Arabidopsis (at 7 days post-germination). Each column represents the average value of an individual genotype or transgenic event. Three individual transgenic events per complementation experiment were included. Error bars represent standard errors. All data were analysed for significance using one-way ANOVA multiple comparisons with the control plants (Col-0, *csld3* or *csld5*) as the main factor. Unless indicated, the treatments showed significant differences (ns, not significant).

AtCslD3 under the *Ubiquitin10* promoter (Figure 6g). However, the *csld3* phenotype was not rescued in the *csld3*¦pUbq10::HvCslF3 transgenic plants (Figure 6e). Interestingly, even though the majority of root hairs were aborted in *csld3* plants, successful root hair initiation was observed occasionally, especially in the more mature parts of the roots. Moreover, in *csld3* plants expressing *HvCslF3*, the number of root hair cells increased, from an average of 24 cells in *csld3* to 32 cells in *csld3*¦pUbq10::HvCslF3 transgenic plants, whereas the root hair density of the lines complemented with *AtCslD3* remained closer to that of the WT (Figure 7b). No significant difference in other aspects of seedling development was observed between the *csld3* and the complemented plants.

The mutant phenotype of *csld3* is epistatic to *csld5*, where the latter mutant is able to initiate root hair formation, but subsequent elongation is disrupted, suggesting the two genes act in the same pathway (Yin et al., 2011). Figure 6(c) illustrates the short root hair phenotype of the *csld5* mutant. Remarkably, transgenic *csld5* plants expressing *HvCslF3* restored root hair lengths to 0.37 mm when driven by the *Ubiquitin10* promoter. The average lengths of root hairs were similar to those observed in the plants complemented with *AtCslD5* (Figure 7a). This result highlights a potentially conserved (or redundant) cross-species function of the *HvCslF3* and *AtCslD5* genes during root hair elongation. Also, similar to the Col-0 plants that express *HvCslF3*, the complemented *csld5* plants exhibited an increased number of root hairs (1.4- to 1.9-fold) compared with Col-0 and *csld5* plants (Figure 7b). Therefore, the expression of *HvCslF3* in Arabidopsis not only contributes to root hair elongation but also drives a gain-of-function phenotype characterized by an increased number of root hairs.

Abnormal trichoblast cell fate is evident in Arabidopsis roots expressing *HvCslF3*

Differences in the patterning of root hair and non-hair cells are found between species (Salazar-Henao et al., 2016). Figure 8 summarizes the position-dependent root hair pattern observed on the root surface of Col-0, *csld3*, *csld5* and *AtCslD3/5* complemented plants, where trichoblasts and atrichoblasts were arranged in cell file patterns. In Arabidopsis plants expressing *HvCslF3*, the arrangement of the root hair cells was disrupted, with the root hairs frequently emerging from adjacent epidermal cells (Figure 8d–f). The transverse view of the reconstructed root sections indicated no change in cellular organization in the cortical cells. However, epidermal cells in contact with only one cortical cell were able to form root hairs (Figure 9). Such observations suggest *HvCslF3* alters pathways that regulate epidermal cell fate determination in Arabidopsis.

DISCUSSION

HvCslF3 is required for normal root growth in barley

The plant cell wall is an important component of root development, contributing to growth, flexibility, elongation and reinforcement as cells exit the meristem and differentiate into various tissues (Houston et al., 2016). The *HvCslF3* gene belongs to a family of putative *cellulose-synthase-like* GT2 enzymes that includes *HvCslF6*, the major determinant

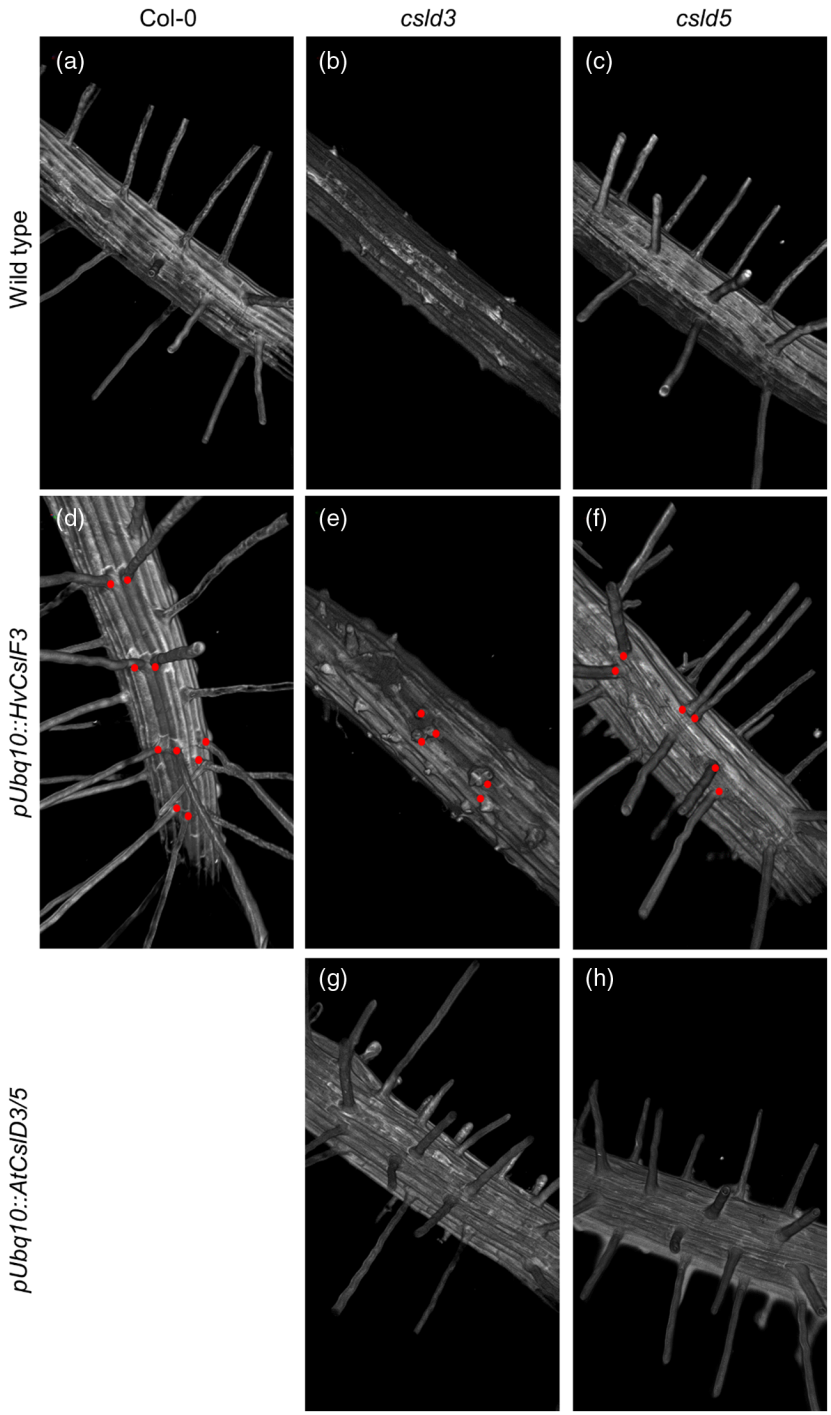

Figure 8. Expression of *HvCslF3* altered the pattern of root hair cell determination in Arabidopsis. Three-dimensnal reconstructed view of root surfaces using Lightsheet microscopy. Red dots indicate abnormal and altered root hair formation in *HvCslF3*-complemented Arabidopsis.
(a) Col-0 wild type (WT).
(b) *csld3* mutant.
(c) *csld5* mutant.
(d) Col-0 expressing *HvCslF3* driven by the *Ubiquitin10* promoter with abnormal position of root hair emergence.
(e) *HvCslF3*complemented *csld3* mutants: the mutant phenotype was not restored but root hairs emerged from abnormal epidermal cells.
(f) *HvCslF3*-complemented *csld5* mutants with restored root hair development and abnormal root hair positions.
(g) *AtCslD3*-complemented *csld3* mutants with recovered root hairs.
(h) *AtCslD5*-complemented *csld5* mutant with recovered root hair development.

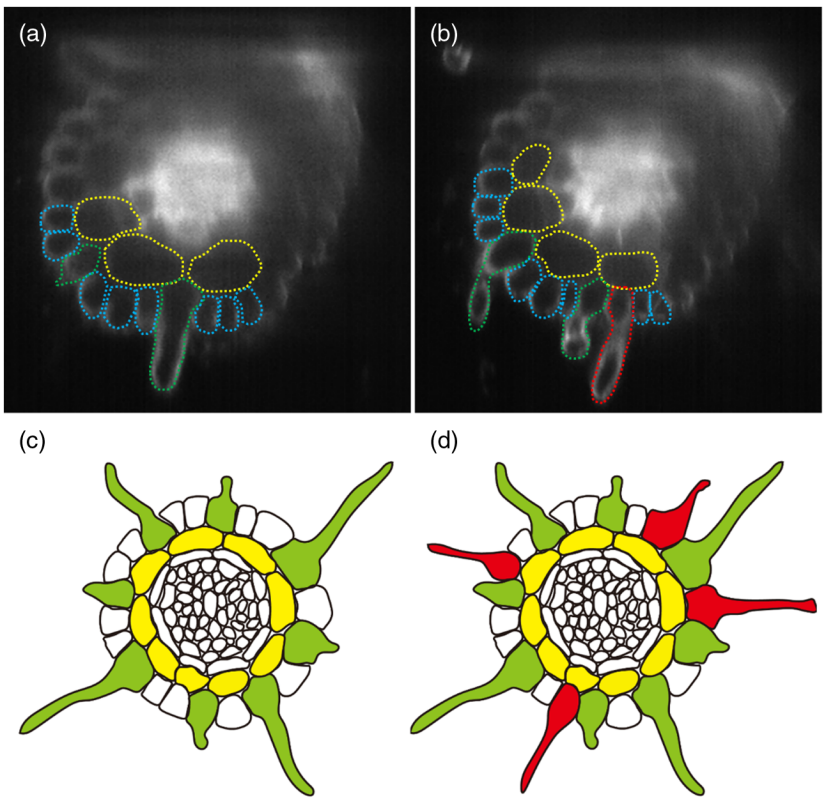

Figure 9. Transverse view of 3D reconstructed roots by Lightsheet microscopy.
(a) Col-0 showing normal root hair emergence from the epidermal cell in direct contact with two cortex cells.
(b) Col-0 expressing *HvCslF3*. Yellow dashed lines outline cortex cells. Blue dashed lines indicate epidermis cells with non-hair fate or the atrichoblasts. Green dashed lines represent epidermal cells with root hair fate or the trichoblasts. Red dashed lines outline abnormal root hair formation, where the root hair emerged from the epidermal cell only in contact with one cortex cell.
(c, d) Schematic diagram showing the root hair organization of the normal plant (c) and Arabidopsis expressing the *HvCslF3* gene (d). Yellow indicates cortical cells, green indicates normal trichoblasts and red indicates abnormal root hair formation.

of (1,3;1,4)-β-glucan biosynthesis (Burton et al., 2008; Schwerdt et al., 2015). Here we show that high expression of *HvCslF3* in the root elongation zone, mainly in cortical and epidermal cells, is required for normal root growth in barley. Cells in this zone undergo rapid division and unidirectional expansion, during which time cell wall assembly and modification are exceptionally important (Somssich et al., 2016). Reduced *HvCslF3* expression is correlated with shorter seminal roots, caused by a shorter elongation zone with a similar number of cells, and leads to negative impacts on overall plant growth. The defects in elongation directly affect the process of cell expansion and result in cells entering maturation earlier than in the WT. This supports a previous hypothesis linking rapid growth to the expression of selected barley *CslF* genes, such as *HvCslF3*, *HvCslF7* and *HvCslF9*, and a possible role in modifying the flexibility and stiffness of extending cell walls (Burton et al., 2008). In the case of *HvCslF3*, this functionality appears to be achieved via the accumulation of (1,4)-β-linked glucoxylan, which showed reduced levels in *RNAi* plants and higher levels in tobacco leaves after transient expression (Little et al., 2019). (1,4)-β-Linked glucoxylan is a non-cellulosic polysaccharide found in the cell walls of the green seaweed *Ulva rigida* (Ray & Lahaye, 1995). Its insoluble linear chain is rich in glucose and xylose, and is predicted to contain a high Glc/Xyl ratio in barley. This molecule is likely to form intermolecular alignments with other cell wall polysaccharides (Little et al., 2019). We speculate that the presence of (1,4)-β-linked glucoxylan in the cell wall matrix of the rapidly expanding cells balances wall flexibility and stiffness. Other polymers detected in this region include callose, pectin and (1,3;1,4)-β-glucan; the former two polymers have been implicated in controlling cell elongation and meristem maintenance (Liu et al., 2020; Müller et al., 2015). Reduced (1,4)-β-linked glucoxylan content may impact the function of these polymers, leading to early maturation of the elongation zone cell walls. The precise location of the polysaccharide remains to be tested in further detail once a suitable antibody can be synthesized.

Reduced cortical cell layers were observed in *HvCslF3-RNAi* barley. Root radial patterning is established during embryogenesis and is maintained in the root meristem by the stem cell niche (Benková & Hejátko, 2008). The determination of cortical cell files is genetically controlled (Chimungu et al., 2014) and influenced by asymmetric periclinal divisions in the meristem (Coudert et al., 2010; Lux et al., 2004). Natural variation in the number of cortex cell layers was also described in *Zea mays* (maize) and rice, and was shown to correlate with drought tolerance (Burton et al., 2013; Chimungu et al., 2014; Coudert et al., 2010). Although the change in cortex morphology is not easy to explain based on the predominant expression pattern of *HvCslF3* in elongating tissues, one possibility is

that the product of *HvCslF3*, possibly (1,4)-β-linked glucoxylan, is essential at low levels for the asymmetric periclinal divisions to establish the radial pattern in the root meristem. This might involve feedback from the wall through specific polysaccharide deposition and changes in the binding of key receptors (Tucker et al., 2018). Alternatively, *HvCslF3* may act as a factor that either directly affects the function of the cortical initials or indirectly induces the expression of genes that control radial patterning, for example the *GRAS* gene family (Cui et al., 2007; Hochholdinger & Zimmermann, 2008; Lim et al., 2000).

Root elongation depends on multiple cell wall-related activities

The transit of root cells to an elongation phase requires alterations in cell shape. Two essential features during this process are turgor pressure and cell wall remodelling. By decreasing the expression of the *HvCslF3* gene, barley exhibited traits, including shorter and thinner roots and altered root hair development, that led to reduced root surface area. These may limit water uptake, which is the main determinant of turgor pressure (Guerriero et al., 2014; Petricka et al., 2012). In terms of the remodelling of cell walls, many genes related to wall loosening and polysaccharide synthesis have been identified in elongating tissues (Markakis et al., 2012; Yang et al., 2011). These include peroxidase, AGPs, xyloglucan hydrolases, pectin synthases and hydrolases, and *CesA*-related genes (Bringmann et al., 2012; Guerriero et al., 2014; Hématy & Höfte, 2006). In rice and *Glycine max* (soybean), the cell wall loosening gene *EXP1* is specifically expressed in the elongating epidermal and underlying cell layers, and induces cell elongation in secondary root initials and transgenic tobacco roots (Lee et al., 2003; Yang et al., 2006). In rice, the increased expression of *OsCslF2* (which shares closest homology with barley *HvCslF4* and *HvCslF11*) was reported in elongating root tips under water stress (Yang et al., 2006). Indeed, changes in root cell elongation and short-root phenotypes have been described in mutants with irregular cellulose, pectin, and mannan synthesis and accumulation (Arioli et al., 1998; McCartney et al., 2003; Passardi et al., 2006; Yin et al., 2011). A common feature of short-root cereal mutants is defective cortical cell elongation, which is also found in *HvCslF3-RNAi* plants. Considering the specificity of *HvCslF3* expression in the elongating cortical and epidermal cells, and its correlation with (1,4)-β-linked glucoxylan concentration, we suggest that this is one of several cell wall components that may interact to regulate cell elongation in barley root cells.

A role for *HvCslF3* in root hair patterning, independent of *CslD* genes

The development of root hairs requires multiple gene networks in response to hormonal and environmental signals. Shibata and Sugimoto (2019) reviewed the regulatory network of Arabidopsis root hair development, focusing mainly on transcription factors and environmental responses. For simplicity, root hair development can be divided into two main phases: phase 1, specification/initiation; and phase 2, growth/elongation. To date, the proposed cell fate determination model (phase 1) involves mainly hormone and transcription factor regulation, whereas cell wall remodelling is thought to be more important in the later stages of root hair development (phase 2), involving polysaccharide rearrangement and elongation (Shibata & Sugimoto, 2019). Here we show that selected *Csl* genes can affect both processes, influencing both the initiation and the growth of root hairs.

In terms of root hair elongation, the overexpression of *HvCslF3* in Col-0 plants led to a significant increase in root hair length. Complementation experiments with *HvCslF3* and *AtCslD3/5* in *csld* mutants induced similar effects. There are several possible explanations for the appearance of longer root hairs in transgenic Arabidopsis in the present study. *AtCslD3/5* and *HvCslF3* may function with *ROOT HAIR SPECIFIC* (*RHS*) genes that synthesize specific cell wall polysaccharides to stimulate pathways promoting cell elongation. Consistent with this, studies on rice and poplar have identified *OsCslD1* (Kim et al., 2007) and *PtrCslD2* (Peng et al., 2019) as members of the *RHS* group, along with other genes regulating cell wall loosening (Hwang et al., 2016). Alternatively, *AtCslD3/5* and *HvCslF3* may alter the expression of *RHS* genes to enhance root hair elongation. Finally, but not mutually exclusively, the *Ubiquitin10* promoter may have uncoupled the cell elongation pathway from endogenous negative *RHS* regulators, leading to the prolonged function of *AtCslD3/5* and *HvCslF3* in promoting cell growth. Although it was not attempted in this study, future research might focus on the molecular pathways impacted by *HvCslF3* overexpression in Arabidopsis.

To date, it has been reported that the *CslD* gene family, rather than the *CslF* genes, show direct involvement in root hair emergence. Although *HvCslF3* promoted root hair elongation in Arabidopsis, its expression in Col-0 plants had no impact on the emergence of root hairs, and could not rescue the aborted root hairs in *csld3* mutants. This suggests that *AtCslD3* is a key determinant for the initiation of root hairs, whereas the product of the *HvCslF3* gene functions downstream of *AtCslD3*. This is consistent with a previous study on the Arabidopsis *csld2/3/5* double and triple mutants, where the root hairs could only be restored in the presence of the *AtCslD3* gene (Yin et al., 2011). The predicted model of the *AtCslD3*–*HvCslF3* relationship is similar to the known *AtCslD2/3/5* regulation network, where the different CslD proteins cooperate with the AtCslD3 protein as the core component.

Consistent with this hypothesis, we also presented the remarkable evidence that *HvCslF3* rescued the *csld5* mutant phenotype. Although it is unclear whether this rescue relates to identical biochemical activity, it possibly reflects an ancestral function conserved between *HvCslF3* and *AtCslD5* in regulating root hair elongation after emergence. Curiously, in contrast to Little et al. (2019), Arabidopsis roots overexpressing *HvCslF3* do not show any detectable (1,4)-β-linked glucoxylan. The definitive biochemical roles of the *CslD* genes are poorly understood, except for the detection of mannan synthase activity in Arabidopsis root hairs when *AtCslD2* and *AtCslD3* are simultaneously overexpressed, whereas the function of *AtCslD5* remains unknown (Yin et al., 2011). In barley and rice, *CslD* genes (*HvCslD2* and *OsCslD4*) (Li et al., 2009; Douchkov et al., 2016) have been implicated in callose and cellulose synthesis. Apart from the production of (1,3;1,4)-β-glucan (*CslF6*) and (1,4)-β-linked glucoxylan (*HvCslF3* and *HvCslF10*), no evidence has been shown to suggest that the *CslF* genes are involved in the synthesis of mannan, callose or cellulose. It seems likely that the HvCslF3 and AtCslD5 proteins are involved in the synthesis of different polysaccharides that share similar properties in promoting cell elongation, enabling both to recover the mutant phenotype of *csld5*.

Despite these functional similarities in root hair elongation, distinct roles were revealed for *HvCslF3* and *AtCslD5* in epidermal cell fate determination. Compared with root hair cells, the non-hair cells exhibit early vacuole development and longer cell length (Masucci et al., 1996; Shibata & Sugimoto, 2019). The morphology of non-hair cells in *csld5* complementation lines expressing *AtCslD5* remained unaffected. However, the distance between root hairs was notably reduced. This suggests a negative effect on the length of root hair-forming cells induced by the overexpression of *AtCslD5*; thus, the root hair density increased with normal epidermal cell fate. In contrast, the number of root hairs in *HvCslF3* overexpression plants increased as a consequence of disrupted epidermal cell fate determination, as evidenced by the disordered root hair patterns. The maintenance of non-root hair cell fate is regulated by many genes and protein complexes, such as the *WEREWOLF* gene and the *GLABRA2* transcription factors (Lee & Schiefelbein, 1999). The alteration of epidermal cell fate observed in Arabidopsis roots expressing *HvCslF3* suggested the pathways that control the status of epidermis cells were disturbed by the product of *HvCslF3*. The activation of *RHD6* is required to switch a normal epidermal cell to root hair. This is achieved by the movement of the CPC–TRY–ETC1 protein complex from non-hair cells to the adjacent cell. However, whether the disruption brought by *HvCslF3* impacts transcription factor movement, protein complexes or downstream regulatory mechanisms requires further investigation.

EXPERIMENTAL PROCEDURES

Plant material preparation

An *HvCslF3* fragment of 402 bp was amplified from cDNA generated from a selection of barley tissues, including leaves, roots and developing endosperm, using the primers F3FRAG5 (5′-GGGCAAGCAGTGGTATCAACGCAG-3′) and F3FRAG3 (5′-GTTGTGCTTGATGCGCCATACGAAG-3′). The amplified fragment lies close to the 5′ end of the open reading frame and was selected on the basis of minimal homology with other barley *CslF* cDNA sequences. The fragment was sequenced and inserted into the pCR8®/GW/TOPO/TA vector. Correct inserts were transferred into the Gateway-compatible hairpin vector pTOOL1 (obtained from the (now ended) Australian Centre for Plant Functional Genomics) using an LR clonase reaction (Invitrogen, now ThermoFisher Scientific), according to the manufacturer's instructions. The resultant RNAi construct, pRB437, targeting *HvCslF3* by dsRNAi, was transformed into *Agrobacterium tumefaciens* AGL1 and used for transformation of the barley cultivar Golden Promise, as described earlier (Burton et al., 2011).

Seeds of the barley cultivar Golden Promise and homozygous *HvCslF3-RNAi* lines (#27, #29, #30; pTOOL1::pRB437) were harvested from glasshouse-grown plants and used in the present experiments. Prior to sowing, all seeds were surface-sterilized in 20% (v/v) sodium hypochlorite solution for 10 min, then rinsed with MilliQ water five times before pre-germination overnight. Root material from germinated seeds was harvested according to the requirements of the different experiments.

For soil-grown Arabidopsis, seeds were stratified at 4°C for 48 h and moved into growth chambers (16-h day/8-h night under 23°C). For growth medium-grown Arabidopsis, seeds were surface-sterilized with 70% (v/v) ethanol containing Triton X-100 (0.01% v/v) for 2 min, followed by a treatment with 5% (v/v) sodium hypochlorite for 8 min. Seeds were washed with sterile distilled water four times before being sown on growth medium (1% agar, 2.22 g L^{-1} MS basal salts, pH 5.8). Plates were sealed with micropore tape and stratified at 4°C for 48 h before being moved into a growth chamber (with 24 h of daylight, 21°C). Plates were kept vertically.

RNA extraction and cDNA synthesis

Plate-germinated barley seeds were kept in the dark for 5 days. Whole root tip (1 cm) and dissected root tips (0–1, 1–2, 3–5 and 5–10 mm from the tips) were harvested using a razor blade, collected in tubes pre-chilled in liquid nitrogen and stored at –80°C before processing. The dissected regions represent meristem, elongation, young maturation and old maturation zones of root tips. The Spectrum Plant Total RNA Kit (Sigma-Aldrich, https://www.sigmaaldrich.com) was used to extract total RNA according to the protocol provided by the manufacturer. DNA residues were removed using the TURBO DNA-free kit (Ambion, now ThermoFisher Scientific, https://www.thermofisher.com). The SuperscriptIII Reverse Transcriptase kit (Invitrogen, now ThermoFisher Scientific) was used to synthesize cDNA following the manufacturer's instructions, except that during the final extension step, only 0.25 μl of enzyme was added. Once synthesized, the cDNA samples were tested with the *HvGAPDH* (HORVU6Hr1G054520) control gene primers to ensure the quality of reverse transcription.

Quantitative polymerase chain reaction (qPCR)

The primers used in the present study are listed in Table S1. Primers were designed using PRIMER3 aiming to include the end of the

coding sequences to the 3′-UTRs of each gene. qPCR was performed following Burton et al. (2004). The raw transcript abundance data were normalized against normalization factors calculated according to the transcript levels of housekeeping genes (*HvGAPDH*, HORVU6Hr1G054520; *HvTubulin*, HORVU1Hr1G081280; *HvHSP70*, HORVU5Hr1G113180; *HvCyclophilin*, HORVU6Hr1G012570) (Vandesompele et al., 2002). The data shown are from representatives of three replicate experiments.

mRNA *in situ* hybridization

Fresh barley (cv. Golden Promise) root tips (2 cm) at 5 dpg were harvested and fixed in formalin–acetic acid–alcohol (FAA) (50% v/v 100% ethanol, 5% v/v glacial acetic acid, 25% v/v 16% paraformaldehyde (electron microscopy grade), 20% v/v diethyl pyrocarbonate (DEPC)-H_2O, 0.1% v/v Tween 20). Fixation was performed on ice for 2 h, including 15 min of vacuum infiltration followed by two 10-min washes in 70% ethanol/DEPC-H_2O, and then stored at 4°C overnight. The samples were dehydrated and cleared with a series of ethanol and HistoChoice® (Sigma-Aldrich, https://www.sigmaaldrich.com) washes before being embedded in molten paraffin wax. The paraffin wax blocks with the root samples were sectioned at 7-μm thickness using a microtome (Leica Microsystems, https://www.leica-microsystems.com) and mounted onto poly-L-lysine-coated slides.

Digoxigenin-labelled antisense and sense probes were synthesized according to Yang et al. (2018). The probes specific to *HvCsIF3* were amplified from Golden Promise root cDNA, using primers fused with the T7 promoter sequence at the 5′ end to allow *in vitro* transcription. The probes were designed to recognize the end of the coding sequence and the 3′-UTR of each gene. The barley *histone H4* gene was used as a positive control. The *in situ* hybridization and detection were performed using the InsituPro VSi robot (Intavis, https://intavispeptides.com) with the protocol described by Zeng et al. (2017).

Morphological measurements on barley roots

For seminal root length and root hair quantification, surface-sterilized and pre-germinated seeds (WT, #27, #29, #30) were placed onto 1% agar plates (pH 5.8), embryo side down. Plates were kept vertically in a growth chamber (16-h day/8-h night, 23°C) to allow root growth. The growth of seminal roots was traced daily for 7 days, at the approximately same time every day. The data shown are the average of measurements for 12 seedlings. Root tips of 7-dpg seedlings were photographed using a Zeiss Stemi SV 6 microscope (Zeiss, https://www.zeiss.com) to determine the root hair number on the surface of the root tips. Only the seminal roots growing flat on the agar surface were selected for the measurements. The number of root hairs was determined using FIJI IMAGEJ (https://fiji.sc). The measurements were made on the surface of approximately 40-mm root tips, on a section of the root region at 5 mm. The root hair numbers were calculated from the average of 10 seminal root tips per barley line.

For root clearing with Hoyer's solution, barley seeds were germinated on a sealed Petri dish for 5 days at room temperature (20-22°C) in the dark. Fresh seminal root tips were collected and fixed in freshly prepared FAA, as described above. The dehydration and clearing protocols were performed as described by Wilkinson and Tucker (2017). The cleared specimens were photographed using a Zeiss Axio Imager M2 microscope and an AxioCam MR R3 camera under bright field, and processed with the Zeiss ZEN imaging software.

Root-bending assays were performed by placing surface-sterilized pre-germinated seeds on the surface of 1% agar medium (pH 5.8) in Petri dishes. The plates were positioned vertically in a growth chamber and kept in the dark at 23°C for 3 days. They were subsequently rotated by 90° to induce gravity sensing. Images were recorded at 0, 0.5, 3, 9, 12 and 24 h post gravistimulus and imported into FIJI IMAGEJ for measurement of the bending angles. At least five seedlings per genotype were used.

Analysis of barley root tip morphology by microscopy

Barley seeds were placed on 1% agar (pH 5.8) plates and grown in a growth chamber under controlled conditions (24 h light, 21°C). Seminal root tips of 5-dpg seedlings were collected to study the cellular structure and tissue arrangement in the root tips.

To visualize the longitudinal structure of the root tips, 2 cm of the root tips were fixed in freshly prepared 4% paraformaldehyde in PBS (w/v, pH 6.9) for 2 h at room temperature under vacuum infiltration. The fixed tissues were washed with PBS twice before clearing with a ClearSee solution. The protocol for root tissue clearing and staining was adapted from Ursache et al. (2018), with the following modifications: the ClearSee solution was changed every 2 days and samples were cleared for at least 1 week before staining. Direct Yellow 96 (CAS-no. 61725-08-4; Sigma-Aldrich) in the ClearSee solution (0.1% w/v; excitation, 488 nm; emission, 519 nm) was used to stain roots for 2 h under vacuum infiltration. Specimens were stored in ClearSee solution at room temperature before further analysis. The root longitudinal images were taken using the Leica SP8 confocal microscope. The centre of the root tip was captured by *z*-stacks to follow the root cell files from the meristem to maturation. Images were processed and stitched using FIJI IMAGEJ (Schindelin et al., 2012) and PHOTOSHOP (Adobe, https://www.adobe.com) for the measurement of meristem and elongation zone sizes. Photos shown are representative of the images of 10 individual specimens. All data obtained were subjected to analysis of significance using two-way analysis of variance (ANOVA) multiple comparisons (PRISM 7.03; GraphPad, https://www.graphpad.com) with WT as the main factors.

For the transverse imaging, 1.5 cm of fresh seminal root tips were collected and immediately embedded into 3.5% agarose. The solidified agarose blocks were mounted onto a metal specimen holder and sectioned transversely at 100 μm using a vibratome. A staining solution of 0.1% Calcofluor White (excitation, 405 nm; emission, 425–275 nm) was used to stain the cell walls. The sections were photographed with a Leica SP5 inverted confocal microscope. The data were processed using FIJI IMAGEJ (Schindelin et al., 2012) to adjust the brightness. The pictures shown are representatives of 10 root tips per barley line.

Immunolocalization of cell wall polysaccharides in barley root tips

Fresh root tips (5 mm) were collected from barley seedlings (5 dpg) and fixed in TEM fixative in PBS (0.25% glutaraldehyde, 4% paraformaldehyde, 4% sucrose) overnight with at least 1 h of vacuum infiltration. The fixed root tips were rinsed in PBS twice for 8 h. Root tips were then embedded in 4% agarose gel to the desired angle and orientation, and the agarose gels were shaped to cuboid. The following dehydration and LR White Resin embedding steps were carried out according to Burton et al. (2011). Longitudinal sections at 1-μm intervals were sectioned using a Leica Microtome EM UC6 with either a glass or a diamond knife. The sections were mounted onto glass slides and dried on a hot plate at 60°C for at least 1 h. The antibodies specific to (1,3;1,4)-β-glucan, callose, AGP, mannan, arabinoxylan and pectin were used for immunolabelling. The immunolabelling was performed as described by Burton et al. (2011). Images were taken and

processed by an Axio Imager M2 microscope using an AxioCam MR R3 camera and Zeiss ZEN imaging software.

Gene phylogenetic analysis

cDNA sequences of *CslD* and *CslF* members of Arabidopsis (*Arabidopsis thaliana*), tomato (*Solanum lycopersicum*), barley (*H. vulgare*) and rice (*O. sativa* Japonica) were obtained from the ENSEMBL databases (https://www.ensembl.org). Candidate sequences were translated and aligned with the MUSCLE (Edgar, 2004) plug-in for GENEIOUS 8.1.9 (https://www.geneious.com) using default parameters. An unrooted phylogenetic tree was constructed with RAXML 7.2.8 (Stamatakis, 2006) plug-in for GENEIOUS using the WAG+G substitution model. Node support was assessed using 500 rapid bootstrap replicates.

Construct design

The GreenGate cloning system was used to design the constructs (Lampropoulos et al., 2013). The *HvCslF3* (HORVU2Hr1G042350) sequence was amplified from the cDNA of the WT barley cv. Golden Promise. *AtCslD3* (At3g03050) and *AtCslD5* (At1g02730) sequences were obtained from Arabidopsis WT ecotype Col-0 genomic DNA and cDNA, respectively. The *BsaI* recognition sites were mutated silently by PCR (*HvCslF3*, $621^{G\rightarrow A}$; *AtCslD3*, $831^{A\rightarrow G}$; *AtCslD5*, $2532^{A\rightarrow G}$) and the resulting amplified coding sequences were cloned into the GGC000 module. The *Ubiquitin10* promoter was amplified from Col-0 genomic DNA and cloned into the GGA000 to serve as an overexpression module. The assembly of the destination vectors was based on the pGGZ003 module backbone, and the detailed list of the modules used for the construction of the destination vectors is shown in Table S2. At least 150 ng of plasmid was used for each module. The GreenGate reaction for ligation was adapted from Lampropoulos et al. (2013). The ligated plasmids were transformed by electroporation into *Escherichia coli* strain DH5-alpha cells.

Agrobacterium-mediated plant transformation and plant selection

The destination vectors were transformed into *Agrobacterium tumefaciens* strain GV3101. Transformation of Arabidopsis was performed by the floral-dip method, essentially as described by Clough and Bent (1998), except that the inflorescences were immersed in *Agrobacterium* suspension for 1 min and the low light/dark treatment after dipping was omitted. Each construct was dipped in three Arabidopsis background genotypes: Col-0, *csld3* (SALK_112105C) and *csld5* (SALK_002118C). The above SALK lines were obtained from the Nottingham Arabidopsis Stock Centre (NASC, https://arabidopsis.info).

The harvested T_0 seeds were subsequently surface-sterilized in 70% (v/v) ethanol and 5% (v/v) sodium hypochlorite, then washed with sterile distilled water before sowing. The selection medium consisted of 2.2 g L^{-1} MS medium containing 1% agar at pH 5.8, with the addition of 40 μg ml^{-1} hygromycin B for selection. Seeds were stratified at 4°C for 48 h before being transferred into a growth chamber for 6 h of light incubation at 21°C to stimulate germination. The plates were wrapped in aluminium foil and kept at 21°C for 3 days for the selection of elongated hypocotyls. Confirmed transgenic seedlings were transferred onto growth medium without hygromycin B and grown for at least 3 weeks before being transferred into soil. Three independent homozygous events for each transformation were selected and used for the root phenotyping experiments.

Analysis of Arabidopsis root morphology

Arabidopsis seeds were sterilized as described above and plated on growth medium. Seeds were stratified at 4°C for 48 h and kept in controlled condition chambers for 7 days prior to analysis. A Stemi SV6 microscope (Zeiss) was used to photograph the root tips. To quantify the number of root hairs and measure the root hair length, the photographs were processed using FIJI IMAGEJ (Schindelin et al., 2012) and ZEN. Data represent the average of at least three independent transgenic events with five replications each. All data obtained for root hair number and length were subjected to analysis of significance using one-way ANOVA multiple comparisons (PRISM 7.03) with Col-0, *csld3* or *csld5* as the main factors.

A 1-cm sample of root tip was collected from the above materials and embedded in 1% agarose in microfibre glass tubes. The position of the root samples was adjusted using a sterilized needle. The microfibre glass tubes were inserted vertically into the sample imaging chamber of the light-sheet fluorescence microscope (Zeiss Z1). The set-up of the microscope chamber was described by von Wangenheim et al. (2017), with the following modifications. The solvent exchange unit was disabled and the imaging chamber was filled with distilled water instead of Arabidopsis growth medium. Once the sample position was verified through the camera, the agarose gel containing the root sample was pushed out using the piston inside the microfibre glass tube, with the excess agarose gel remaining inside the tube to hold the sample position in the imaging chamber. The *z*-stack images of whole roots were captured under 10× magnification and UV light using ZEN. The 3D reconstruction of whole roots was performed using VISION4D (Arivis, https://www.arivis.com). The photographs represent the result of at least five replications from each individual transgenic event and control plants.

Enzymatic hydrolysis, oligosaccharide fractionation and (1,4)-β-linked glucoxylan quantification

For the collection of barley root material, surface-sterilized seeds were soaked in water overnight before being placed into germination pouches (Phytotc, https://www.phytotc.com). Water was supplied as required and 1 cm of root tip was harvested at day 5 using a razor blade. For the collection of Arabidopsis material, surface-sterilized Arabidopsis seeds were plated on growth medium and stratified at 4°C for 48 h. The plates were placed vertically in a growth chamber, and the seedlings were harvested after 4 weeks of growth. Fresh barley and Arabidopsis materials were transferred into liquid nitrogen pre-chilled tubes and freeze-dried overnight. Dried materials were then ground with a tissue grinder (Retsch, https://www.retsch.com) and kept at room temperature in a dry environment. The alcohol insoluble residues (AIRs) of each sample were extracted according to Little et al. (2019), except that the materials were resuspended and washed in a sequence of 1 ml of 70% ethanol, 100% ethanol and 100% acetone, and then dried under vacuum (centrifugal evaporator). AIR samples (5 mg) were hydrolysed with cellulase (endo-glucanase, *Trichoderma longibrachiatum*, E-CELTR; Megazyme, https://www.megazyme.com). The AIR samples were mixed with 20 μl of 100% ethanol before adding the hydrolysis buffer (0.7% v/v E-CELTR and 2% v/v 1 M sodium acetate in water). The mixtures were kept at 40°C for 18 h, and rotated gently on a slow rotation shaker. The hydrolysed samples were centrifuged for 10 min at 10 000 ***g*** and the supernatants were fractionated on graphitized carbon SPE cartridges (1 ml/50 mg, Bond Elute; Agilent, https://www.agilent.com). The cartridges were pre-treated with 1 ml of 100% acetonitrile and 1 ml

of water. Supernatant (1 ml) was loaded onto the cartridges, which were washed in water. Elution was performed with 8% acetonitrile followed by 55% acetonitrile to extract the remaining oligosaccharides. The oligosaccharide fractions were dried on a centrifugal evaporator and redissolved in 50 μl of water. A Dionex ICS-5000 (ThermoFisher Scientific) with a CarboPac PA200 (3 × 250 mm) column paired with guard (3 × 50mm) was used to analyse the fractions (Little et al., 2019), with modifications to solvents (A, 0.1 M sodium hydroxide; B, 0.1 M sodium hydroxide, 1 M sodium acetate; C, water; D, 20 mM sodium hydroxide, 100 mM sodium acetate) and gradients (Figure S6), in order to optimize the separation of Glc*p*-(1,4)-β-Xyl*p* from xylobiose and Xyl*p*-(1,4)-β-Glc*p* from cellobiose, as well as the separation from larger oligosaccharides that were eluted later in the chromatogram. A 10-μl portion of each sample was injected using the Pushpartial_Is mode into a 25-μl injection loop. Peak areas were converted into concentrations using the calibration curves of Glc*p*-(1,4)-β-Xyl*p* and Xyl*p*-(1,4)-β-Glc*p*. Results show the average of three replicates. All data obtained were subjected to analysis of significance using two-way ANOVA multiple comparisons (PRISM 7.03), with WT as the main factor.

ACKNOWLEDGEMENTS

This study was supported by the University of Adelaide and the University of Nottingham joint PhD training programme (Beacon of Enlightenment PhD scholarship to HL) and the Australian Research Council Centre of Excellence in Plant Cell Walls. The authors thank Dr Rohan Singh (University of Adelaide) for his assistance with barley transformation. Open access publishing facilitated by The University of Adelaide, as part of the Wiley - The University of Adelaide agreement via the Council of Australian University Librarians. [Correction added on 12 May 2022, after first online publication: CAUL funding statement has been added.]

AUTHOR CONTRIBUTIONS

HL, MRT, MJB, LB and VB conceptualized the study. RAB provided the barley transgenic material. HL, NJS, JL, XY, CM, JS and RF performed the experiments and analysed the data. HL wrote the first draft of the manuscript with support and further input from MRT, MJB and VB.

CONFLICT OF INTEREST

The authors have no conflicts of interest associated with this work.

DATA AVAILABILITY STATEMENT

All relevant data can be found within the manuscript and its supporting information.

SUPPORTING INFORMATION

Additional Supporting Information may be found in the online version of this article.

Figure S1. Negative effects on root development throughout vegetative growth caused by reduced *HvCslF3* expression.

Figure S2. Root bending sensitivity assay.

Figure S3. Immunolabelling images showing the deposition of major cell wall polysaccharides in the root tips of WT and *HvCslF3-RNAi* plants.

Figure S4. Phylogenetic tree of the *CslF* and *CslD* gene families in two monocot and two eudicot species.

Figure S5. Quantitative Dionex analysis of oligosaccharides in the clarified solutions of E-CELTR hydrolysed Arabidopsis seedlings samples.

Figure S6. Solvent gradient methods used for (1,4)-β-linked glucoxylan quantification.

Table S1. Primers used in this study.

Table S2. Assembly of GreenGate destination vectors for the Arabidopsis complementation experiments.

REFERENCES

Arioli, T., Peng, L., Betzner, A.S., Burn, J., Wittke, W., Herth, W. *et al.* (1998) Molecular analysis of cellulose biosynthesis in Arabidopsis. *Science*, **279**, 717–720.

Benková, E. & Hejátko, J. (2008) Hormone interactions at the root apical meristem. *Plant Molecular Biology*, **69**, 383–396.

Bringmann, M., Li, E., Sampathkumar, A., Kocabek, T., Hauser, M.T. & Persson, S. (2012) POM-POM2/cellulose synthase interacting1 is essential for the functional association of cellulose synthase and microtubules in Arabidopsis. *The Plant Cell*, **24**, 163–177.

Burton, A.L., Brown, K.M. & Lynch, J.P. (2013) Phenotypic diversity of root anatomical and architectural traits in *Zea* species. *Crop Science*, **53**, 1042–1055.

Burton, R.A., Collins, H.M., Kibble, N.A.J., Smith, J.A., Shirley, N.J., Jobling, S.A. *et al.* (2011) Over-expression of specific HvCslF cellulose synthase-like genes in transgenic barley increases the levels of cell wall (1,3;1,4)-β-D-glucans and alters their fine structure. *Plant Biotechnology Journal*, **9**, 117–135.

Burton, R.A., Jobling, S.A., Harvey, A.J., Shirley, N.J., Mather, D.E., Bacic, A. *et al.* (2008) The genetics and transcriptional profiles of the cellulose synthase-like HvCslF gene family in barley. *Plant Physiology*, **146**, 1821–1833.

Burton, R.A., Shirley, N.J., King, B.J., Harvey, A.J. & Fincher, G.B. (2004) The CesA gene family of barley. Quantitative analysis of transcripts reveals two groups of co-expressed genes. *Plant Physiology*, **134**, 224–236.

Burton, R.A., Wilson, S.M., Hrmova, M., Harvey, A.J., Shirley, N.J., Medhurst, A. *et al.* (2006) Cellulose synthase-like CslF genes mediate the synthesis of cell wall (1, 3; 1, 4)-β-D-glucans. *Science*, **311**, 1940–1942.

Chimungu, J.G., Brown, K.M. & Lynch, J.P. (2014) Reduced root cortical cell file number improves drought tolerance in maize. *Plant Physiology*, **166**, 1943–1955.

Clough, S.J. & Bent, A.F. (1998) Floral dip: a simplified method for *Agrobacterium*-mediated transformation of *Arabidopsis thaliana*. *The Plant Journal*, **16**, 735–743.

Cocuron, J.-C., Lerouxel, O., Drakakaki, G., Alonso, A.P., Liepman, A.H., Keegstra, K. *et al.* (2007) A gene from the cellulose synthase-like C family encodes a β-1, 4 glucan synthase. *Proceedings of the National Academy of Sciences of the United States of America*, **104**, 8550–8555.

Coudert, Y., Périn, C., Courtois, B., Khong, N.G. & Gantet, P. (2010) Genetic control of root development in rice, the model cereal. *Trends in Plant Science*, **15**, 219–226.

Cseh, A., Soós, V., Rakszegi, M., Türkösi, E., Balázs, E. & Molnár-Láng, M. (2013) Expression of HvCslF9 and HvCslF6 barley genes in the genetic background of wheat and their influence on the wheat β-glucan content. *Annals of Applied Biology*, **163**, 142–150.

Cui, H., Levesque, M.P., Vernoux, T., Jung, J.W., Paquette, A.J., Gallagher, K.L. *et al.* (2007) An evolutionarily conserved mechanism delimiting SHR movement defines a single layer of endodermis in plants. *Science*, **316**, 421–425.

De Lorenzo, G., Ferrari, S., Giovannoni, M., Mattei, B. & Cervone, F. (2019) Cell wall traits that influence plant development, immunity and bioconversion. *Plant Journal*, **97**, 134–147.

Dhugga, K.S., Barreiro, R., Whitten, B., Stecca, K., Hazebroek, J., Randhawa, G.S. *et al.* (2004) Guar seed β-mannan synthase is a member of the cellulose synthase super gene family. *Science*, **303**, 363–366.

Doblin, M.S., Kurek, I., JacobWilk, D. & Delmer, D.P. (2002) Cellulose biosynthesis in plants: from genes to rosettes. *Plant Cell Physiology*, **43**, 1407–1420.

Doblin, M.S., Pettolino, F.A., Wilson, S.M., Campbell, R., Burton, R.A., Fincher, G.B. *et al.* (2009) A barley cellulose synthase-like CslH gene mediates (1, 3; 1, 4)-β-D-glucan synthesis in transgenic Arabidopsis. *Proceedings of the National Academy of Sciences of the United States of America*, **106**, 5996–6001.

Douchkov, D., Lueck, S., Hensel, G., Kumlehn, J., Rajaraman, J., Johrde, A. *et al.* (2016) The barley (*Hordeum vulgare*) cellulose synthase-like D2 gene (HvCslD2) mediates penetration resistance to host-adapted and nonhost isolates of the powdery mildew fungus. *New Phytologist*, **212**, 421–433.

Edgar, R.C. (2004) MUSCLE: multiple sequence alignment with high accuracy and high throughput. *Nucleic Acids Research*, **32**, 1792–1797.

Garcia-Gimenez, G., Barakate, A., Smith, P., Stephens, J., Khor, S.F., Doblin, M.S. *et al.* (2020) Targeted mutation of barley (1, 3; 1, 4)-β-glucan synthases reveals complex relationships between the storage and cell wall polysaccharide content. *Plant Journal*, **104**, 1009–1022.

Goubet, F., Barton, C.J., Mortimer, J.C., Yu, X., Zhang, Z., Miles, G.P. *et al.* (2009) Cell wall glucomannan in Arabidopsis is synthesised by CSLA glycosyltransferases, and influences the progression of embryogenesis. *The Plant Journal*, **60**, 527–538.

Guerriero, G., Hausman, J.-F. & Cai, G. (2014) No stress! Relax! Mechanisms governing growth and shape in plant cells. *International Journal of Molecular Sciences*, **15**, 5094–5114.

Hazen, S.P., ScottCraig, J.S. & Walton, J.D. (2002) Cellulose synthase-like genes of rice. *Plant Physiology*, **128**, 336–340.

Hématy, K. & Höfte, H. (2006) Cellulose and cell elongation. In: Verbelen, J.P. & Vissenberg, K. (Eds.) *The expanding cell*. Berlin, Heidelberg: Springer, vol **6**, pp. 33–56. https://doi.org/10.1007/7089_2006_070

Hochholdinger, F. & Zimmermann, R. (2008) Conserved and diverse mechanisms in root development. *Current Opinion in Plant Biology*, **11**, 70–74.

Houston, K., Tucker, M.R., Chowdhury, J., Shirley, N. & Little, A. (2016) The plant cell wall: a complex and dynamic structure as revealed by the responses of genes under stress conditions. *Frontiers in Plant Science*, **7**, 984–1001.

Hwang, Y., Lee, H., Lee, Y.S. & Cho, H.T. (2016) Cell wall-associated ROOT HAIR SPECIFIC 10, a proline-rich receptor-like kinase, is a negative modulator of Arabidopsis root hair growth. *Journal of Experimental Botany*, **67**, 2007–2022.

Kim, C.M., Park, S., Je, B.I., Park, S., Park, S., Piao, H.L. *et al.* (2007) OsCSLD1, a cellulose synthase-like D1 gene, is required for root hair morphogenesis in rice. *Plant Physiology*, **143**, 1220–1230.

Kirschner, G.K., Stahl, Y., Von Korff, M. & Simon, R. (2017) Unique and conserved features of the barley root meristem. *Frontiers in Plant Science*, **8**, 1240.

Lampropoulos, A., Sutikovic, Z., Wenzl, C., Maegele, I., Lohmann, J.U. & Forner, J. (2013) GreenGate - a novel, versatile, and efficient cloning system for plant transgenesis. *PLoS One*, **8**, e83043.

Lee, D.K., Ahn, J.H., Song, S.K., Do Choi, Y. & Lee, J.S. (2003) Expression of an expansin gene is correlated with root elongation in soybean. *Plant Physiology*, **131**, 985–997.

Lee, M.M. & Schiefelbein, J. (1999) WEREWOLF, a MYB-related protein in Arabidopsis, is a position-dependent regulator of epidermal cell patterning. *Cell*, **99**, 473–483.

Li, M., Xiong, G., Li, R., Cui, J., Tang, D., Zhang, B. *et al.* (2009) Rice cellulose synthase-like D4 is essential for normal cell-wall biosynthesis and plant growth. *The Plant Journal*, **60**, 1055–1069.

Liepman, A.H., Wilkerson, C.G. & Keegstra, K. (2005) Expression of cellulose synthase-like (*Csl*) genes in insect cells reveals that *CslA* family members encode mannan synthases. *Proceedings of the National Academy of Sciences of the United States of America*, **102**, 2221–2226.

Lim, J., Helariutta, Y., Specht, C.D., Jung, J., Sims, L., Bruce, W.B. *et al.* (2000) Molecular analysis of the SCARECROW gene in maize reveals a common basis for radial patterning in diverse meristems. *The Plant Cell*, **12**, 1307–1318.

Little, A., Lahnstein, J., Jeffery, D.W., Khor, S.F., Schwerdt, J.G., Shirley, N.J. *et al.* (2019) A novel (1, 4)-β-linked glucoxylan is synthesized by members of the cellulose synthase-like F gene family in land plants. *ACS Central Science*, **5**, 73–84.

Little, A., Schwerdt, J.G., Shirley, N.J., Khor, S.F., Neumann, K., O'Donovan, L.A. *et al.* (2018) Revised phylogeny of the cellulose synthase gene superfamily: insights into cell wall evolution. *Plant Physiology*, **177**, 1124–1141.

Liu, X., Cui, H., Zhang, B., Song, M., Chen, S., Xiao, C. *et al.* (2020) Reduced pectin content of cell walls prevents stress-induced root cell elongation in Arabidopsis. *Journal of Experimental Botany*, **72**, 1073–1084.

Lombard, V., Ramulu, H.G., Drula, E., Coutinho, P.M. & Henrissat, B. (2014) The carbohydrate-active enzymes database (CAZy) in 2013. *Nucleic Acids Research*, **42**, D490–D495.

Lux, A., Luxová, M., Abe, J. & Morita, S. (2004) Root cortex: structural and functional variability and responses to environmental stress. *Root Research*, **13**, 117–131.

Markakis, M.N., De Cnodder, T., Lewandowski, M., Simon, D., Boron, A., Balcerowicz, D. *et al.* (2012) Identification of genes involved in the ACC-mediated control of root cell elongation in *Arabidopsis thaliana*. *BMC Plant Biology*, **12**, 208.

Masucci, J.D., Rerie, W.G., Foreman, D.R., Zhang, M., Galway, M.E., Marks, M.D. *et al.* (1996) The homeobox gene GLABRA2 is required for position-dependent cell differentiation in the root epidermis of *Arabidopsis thaliana*. *Development*, **122**, 1253–1260.

McCartney, L., Steeleking, C.G., Jordan, E. & Knox, J.P. (2003) Cell wall pectic (1-4)-β-D-galactan marks the acceleration of cell elongation in the Arabidopsis seedling root meristem. *The Plant Journal*, **33**, 447–454.

Müller, J., Toev, T., Heisters, M., Teller, J., Moore, K.L., Hause, G. *et al.* (2015) Iron-dependent callose deposition adjusts root meristem maintenance to phosphate availability. *Developmental Cell*, **33**, 216–230.

Passardi, F., Tognolli, M., De Meyer, M., Penel, C. & Dunand, C. (2006) Two cell wall associated peroxidases from Arabidopsis influence root elongation. *Planta*, **223**, 965–974.

Peng, X., Pang, H., Abbas, M., Yan, X., Dai, X., Li, Y. *et al.* (2019) Characterization of cellulose synthase-like D (CSLD) family revealed the involvement of PtrCslD5 in root hair formation in *Populus trichocarpa*. *Scientific Reports*, **9**, 1452–1460.

Petricka, J.J., Winter, C.M. & Benfey, P.N. (2012) Control of Arabidopsis root development. *Annual Review of Plant Biology*, **63**, 563–590.

Ray, B. & Lahaye, M. (1995) Cell-wall polysaccharides from the marine green alga *Ulva* "rigida"(Ulvales, Chlorophyta). Extraction and chemical composition. *Carbohydrate Research*, **274**, 251–261.

Richmond, T.A. & Somerville, C.R. (2000) The cellulose synthase superfamily. *Plant Physiology*, **124**, 495–498.

Salazar-Henao, J.E., Vélez-Bermúdez, I.C. & Schmidt, W. (2016) The regulation and plasticity of root hair patterning and morphogenesis. *Development*, **143**, 1848–1858.

Schindelin, J., Arganda-Carreras, I., Frise, E., Kaynig, V., Longair, M., Pietzsch, T. *et al.* (2012) Fiji: an open-source platform for biological-image analysis. *Nature Methods*, **9**, 676–682.

Schwerdt, J.G., MacKenzie, K., Wright, F., Oehme, D., Wagner, J.M., Harvey, A.J. *et al.* (2015) Evolutionary dynamics of the Cellulose Synthase gene superfamily in grasses. *Pant Physiology*, **168**, 968–983.

Shibata, M. & Sugimoto, K. (2019) A gene regulatory network for root hair development. *Journal of Plant Research*, **132**, 301–309.

Somssich, M., Khan, G.A. & Persson, S. (2016) Cell wall heterogeneity in root development of Arabidopsis. *Frontiers in Plant Science*, **7**, 1242–1252.

Stamatakis, A. (2006) RAxML-VI-HPC: maximum likelihood-based phylogenetic analyses with thousands of taxa and mixed models. *Bioinformatics*, **22**, 2688–2690.

Taketa, S., Yuo, T., Tonooka, T., Tsumuraya, Y., Inagaki, Y., Haruyama, N. *et al.* (2011) Functional characterization of barley betaglucanless mutants demonstrates a unique role for CslF6 in (1, 3; 1, 4)-β-D-glucan biosynthesis. *Journal of Experimental Botany*, **63**, 381–392.

Tucker, M.R., Lou, H., Aubert, M.K., Wilkinson, L.G., Little, A., Houston, K. *et al.* (2018) Exploring the role of cell wall-related genes and polysaccharides during plant development. *Plants*, **7**, 42–58.

Ursache, R., Andersen, T.G., Marhavý, P. & Geldner, N. (2018) A protocol for combining fluorescent proteins with histological stains for diverse cell wall components. *The Plant Journal*, **93**, 399–412.

Vandesompele, J., De Preter, K., Pattyn, F., Poppe, B., Van Roy, N., De Paepe, A. *et al.* (2002) Accurate normalization of real-time quantitative RT-PCR data by geometric averaging of multiple internal control genes. *Genome Biology*, **3**(research0034), 0031.

Verhertbruggen, Y., Yin, L., Oikawa, A., Scheller, H.V. & behavior (2011) Mannan synthase activity in the CslD family. *Plant Signaling*, **6**, 1620–1623.

von Wangenheim, D., Hauschild, R. & Friml, J. (2017) Light sheet fluorescence microscopy of plant roots growing on the surface of a gel. *Journal of Visualized Experiments*, **119**, e55044.

Wilkinson, L.G. & Tucker, M.R. (2017) An optimised clearing protocol for the quantitative assessment of sub-epidermal ovule tissues within whole cereal pistils. *Plant Methods*, **13**, 67–76.

Yang, J.L., Zhu, X.F., Peng, Y.X., Zheng, C., Li, G.X., Liu, Y. *et al.* (2011) Cell wall hemicellulose contributes significantly to aluminum adsorption and root growth in Arabidopsis. *Plant Physiology*, **155**, 1885–1892.

Yang, L., Wang, C.C., Guo, W.D., Li, X.B., Lu, M. & Yu, C.L. (2006) Differential expression of cell wall related genes in the elongation zone of rice roots under water deficit. *Russian Journal of Plant Physiology*, **53**, 390–395.

Yang, X., Li, G., Tian, Y., Song, Y., Liang, W. & Zhang, D. (2018) A rice glutamyl-tRNA synthetase modulates early anther cell division and patterning. *Plant Physiology*, **177**, 728–744.

Yin, L., Verhertbruggen, Y., Oikawa, A., Manisseri, C., Knierim, B., Prak, L. *et al.* (2011) The cooperative activities of CSLD2, CSLD3, and CSLD5 are required for normal Arabidopsis development. *Molecular Plant*, **4**, 1024–1037.

Zeng, J., Dong, Z., Wu, H., Tian, Z. & Zhao, Z. (2017) Redox regulation of plant stem cell fate. *The EMBO Journal*, **36**, 2844–2855.